JOURNAL OF GEOPHYSICAL RESEARCH, VOL. 102, NO. B12, PAGES 27,603–27,621, DECEMBER 10, 1997

Uplift of the Transantarctic Mountains and the bedrock beneath the East Antarctic ice sheet

Uri S. ten Brink,[1] Ron I. Hackney,[2,3] Stephen Bannister,[4] Tim A. Stern,[2] and Yizhaq Makovsky[5]

Abstract. In recent years the Transantarctic Mountains (TAM), the largest noncontractional mountain belt in the world, have become the focus of modelers who explained their uplift by a variety of isostatic and thermal mechanisms. A problem with these models is a lack of available data to compare with model predictions. We report here the results of a 312-km-long geophysical traverse conducted in 1993/1994 in the hinterland of the TAM. Using detailed subglacial topography and gravity measurements, we confirm the origin of the TAM as a flexural uplift of the edge of East Antarctica. Using an elastic model with a free edge, we can jointly fit the topography and the gravity with a plate having an elastic thickness of 85 ± 15 km and a preuplift elevation of 700 ± 50 m for East Antarctica. Using a variety of evidence, we argue that the uplift is coincident with a relatively minor tectonic event of transtensional motion between East and West Antarctica during the Eocene rather than the Late Cretaceous rifting event that created the Ross Embayment. We suggest that this transtensional motion caused the continuous plate to break, which created an escarpment that significantly increased the rates of erosion and exhumation. Results from the geophysical traverse also extend our knowledge of the bedrock geology from the exposures within the TAM to the ice covered interior. Our interpretation suggests that the Ferrar flood basalts extend at least 100 km westward under the ice. The Beacon Supergroup of Paleozoic and Mesozoic sediments thins gradually under the ice and its reconstructed thickness is reminiscent of profiles of foreland basins. Finally, there is no indication in the gravity field for an incomplete rebound due to significant melting of the East Antarctic ice sheet since the last glacial period.

1. Introduction

The Transantarctic Mountains (TAM) (Figure 1) with a length of 3500 km and elevations of up to 4500 m [*Robinson and Splettstoesser*, 1984], are one of the major Cenozoic mountain ranges in the world. They are by far the most striking example of a noncontractional mountain belt (i.e., where compression and subduction are not involved). The TAM are characterized by a lack of folding or thrust faulting and are generally described as a gently tilted to block-faulted mountain range (Figure 2). Adjacent to the TAM is a vast submerged region of extended continental crust, the Ross Embayment, which has been dissected by several Mesozoic and Cenozoic age rifts [e.g., *Cooper et al.*, 1991]. Parallel to the TAM and within East Antarctica is the Wilkes subglacial basin, a 200- to 600-km-wide depression which is associated with a 20- to 40-mGal negative gravity anomaly [*Bentley*, 1983; *Crary*, 1963; *Drewry*, 1976]. *Stern and ten Brink* [1989] modeled the geometry of the TAM as an upward flexed cantilevered elastic beam and the Wilkes Basin as the "outer low" resulting from this flexure.

Several uplift mechanisms have been suggested for the Transantarctic Mountains: thermal conduction or advection from the hotter West Antarctic lithosphere to the cooler East Antarctic lithosphere [*Stern and ten Brink*, 1989; *ten Brink and Stern*, 1992; *ten Brink et al.*, 1993], isostatic rebound following normal faulting [*Bott and Stern*, 1992], simple shear extension [*Fitzgerald et al.*, 1986], plastic necking [*Chéry et al.*, 1992] and elastic necking [*van der Beek et al.*, 1994], and rebound in response to erosion [*Stern and ten Brink*, 1989]. The role of ice sheet loading in the uplift was shown to be minimal (100–200 m [*Stern and ten Brink*, 1989]).

However, none of the previous models considered that the initiation of the main phase of uplift was not coincident with the main phase of extension. In addition, new evidence suggests that the isostatic response of the TAM is mechanically decoupled from that in the Ross Embayment. Finally, the uplift is coincident with a possible period of oblique extension or transtension between East and West Antarctica. Hence modeling the flexure of the Transantarctic Mountains as a coupled system with the Ross Embayment, which is subjected to perpendicular extension [*Bott and Stern*, 1992; *Chéry et al.*, 1992; *van der Beek et al.*, 1994], may not be justified. We suggest instead that although lateral heating caused thermal buoyancy since the period of Ross Embayment extension, uplift and denudation were small as long as the plate was continuous. The shear motion in the early Cenozoic, however, may

[1]U.S. Geological Survey, Woods Hole, Massachusetts.
[2]Institute of Geophysics, Victoria University of Wellington, Wellington, New Zealand.
[3]Now at Department of Geology and Geophysics, University of Western Australia, Nedlands, Australia.
[4]Institute of Geological and Nuclear Sciences, Wellington, New Zealand.
[5]Geophysics Department, Stanford University, Stanford, California.

Copyright 1997 by the American Geophysical Union.

Paper number 97JB02483.
0148-0227/97/97JB-02483$09.00

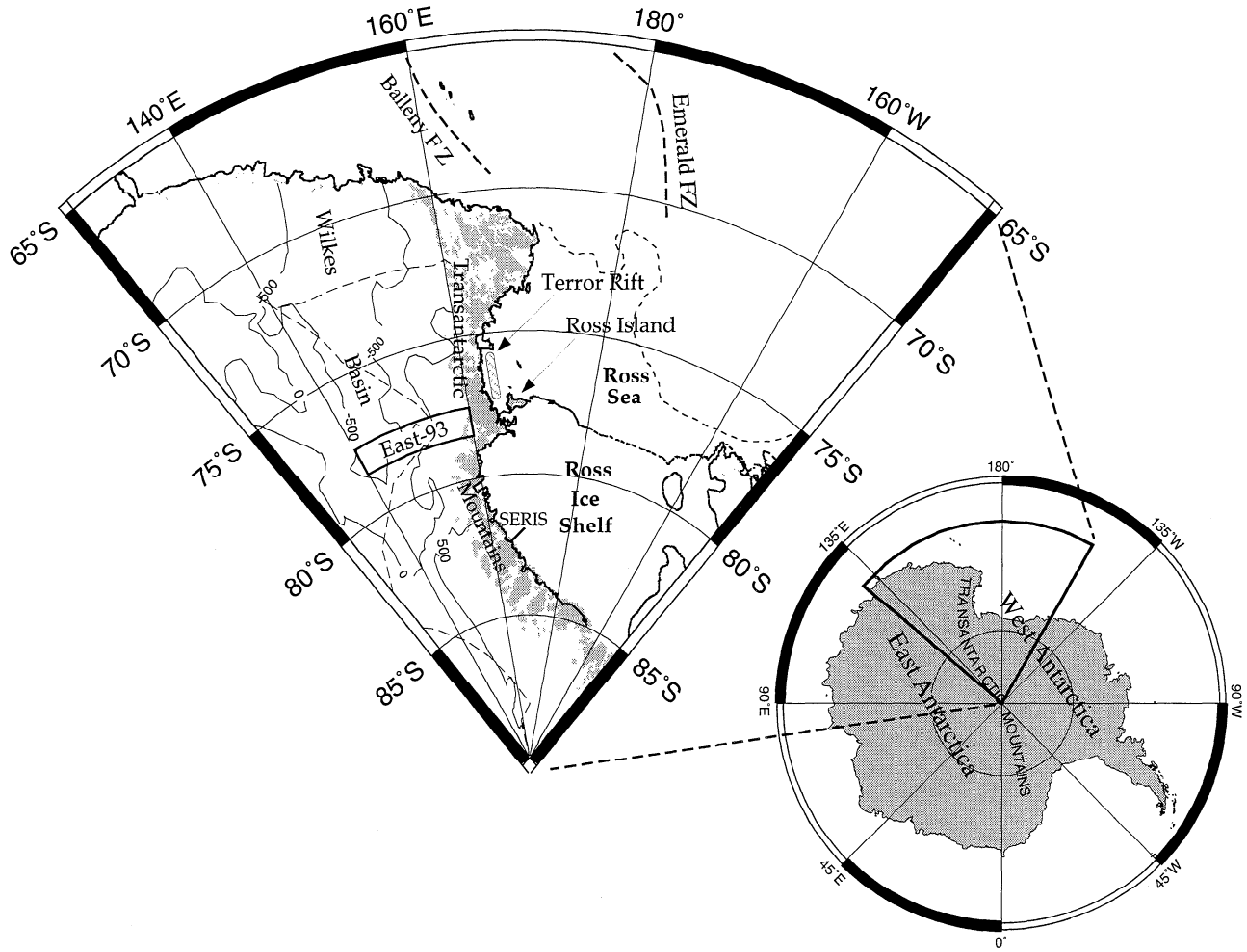

Figure 1. Location map of Antarctica. East Antarctica includes the Transantarctic Mountains (TAM) and the Wilkes Basin. West Antarctica includes the Ross Sea (with the Terror Rift), the Ross Ice Shelf, and Ross Island. Note that in this sector of Antarctica, East Antarctica is in the west and West Antarctica is in the east. Subglacial topography under the ice sheet is drawn at 500-m contour interval [after *Drewry*, 1983]. Shaded area, exposed bedrock; dotted lines, approximate ocean-continent boundary; dashed lines, routes of traverses carried out between 1957 and 1961 [*Crary*, 1963]; heavy line marked SERIS, location of the 1990/1991, seismic experiment across the boundary between East and West Antarctica in the central TAM [*ten Brink et al.*, 1993]; rectangular box, location of EAST93 traverse shown in Figure 3.

have broken the lithosphere along the TAM front, which changed both elevation and the surface slope, and these effects accelerated denudation.

In support of this new model for the origin of the TAM, we report the results of East Antarctic Seismic Traverse 1993 (EAST93) which was carried out across the TAM hinterland during the Austral summer of 1993/1994 by several American and New Zealand institutions. EAST93 was, to our knowledge, the first-ever modern geophysical traverse on the East Antarctic ice sheet, and only one other geophysical traverse was carried out in this area prior to our experiment, the 1958–1959 Victoria Land Traverse [*Crary*, 1963; *Robinson and Splettstoesser*, 1984] (Figure 1). The lack of prior experience in this harsh environment presented several operational and logistical challenges [*ten Brink and Bannister*, 1995]. Nevertheless, for the first time the results provide two data sets along a single profile, topography and gravity, to constrain the models for the uplift of the Transantarctic Mountains. Although the main focus of this paper is the flexural uplift, the results also extend our knowledge of the bedrock geology from the exposed bedrock in the TAM inland under the ice sheet. In this paper, therefore we also consider other diverse problems such as the width of the Ferrar flood basalt province, the lack of evidence for glacial rebound from the last glacial period, the lack of evidence for sedimentary source in the hinterland for Pliocene diatoms which are found in the TAM, and the distribution of Paleozoic sediments in the interior of East Antarctica.

2. Geological Background

2.1. Basement Geology in the TAM

Archean and Proterozoic igneous and metamorphic rocks are exposed all around the perimeter of East Antarctica and are believed to occupy the majority of the hinterland. They are only exposed in one area of the TAM (the Miller Range) where isotopic data and field relationship suggest Late Precambrian thrusting and collision (the Beardmore Orogeny) of

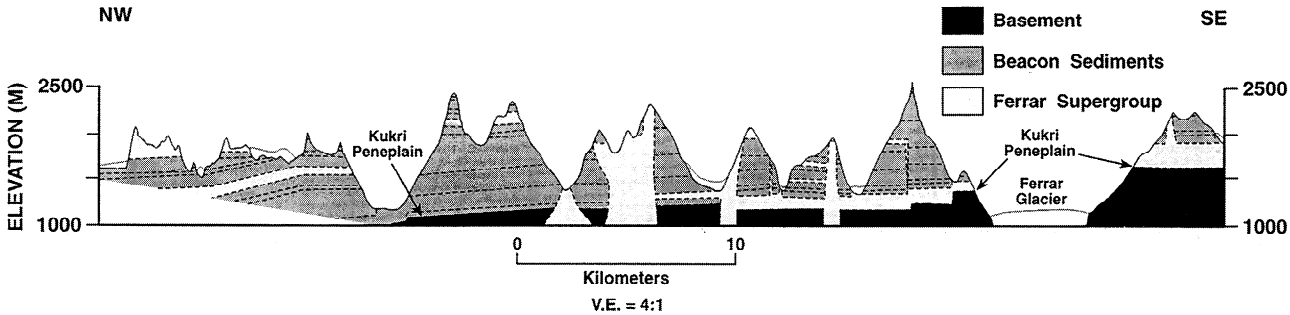

Figure 2. Geological cross section of the TAM [after *McElroy and Rose*, 1987; *Woolfe et al.*, 1989] showing the geological relationship between the crystalline and metamorphic basement (black), the Beacon Supergroup sediments (gray), and the Ferrar flood basalts (light gray and stippled). See Figure 3a for location. The Kukri peneplain is an erosional surface between the basement and the Beacon sediments. Note the absence of compressive deformation within the sediments.

a 1.7 Ga microcontinent onto an hinterland Archean province [*Borg et al.*, 1990]. Low-grade Cambrian metasediments, very thick in places, overlie unconformably the Late Precambrian rocks. The Late Precambrian and Cambrian rocks were metamorphosed and deformed during the Ross Orogeny, 500–530 Ma [*Borg et al.*, 1990]. Granitoid intrusions along almost the entire length of the TAM are associated with this orogeny.

2.2. Sedimentary Section

A Silurian to Early Devonian erosional surface, the Kukri peneplain, separates the crystalline and metamorphosed basement rocks from the overlying Beacon Supergroup (Figure 2). The Beacon Supergroup comprises a 2.7- to 3.5-km-thick undeformed sequence of Devonian to Jurassic age, fluvial, glacial, and shallow marine deposits [*Barrett et al.*, 1986]. *Collinson* [1991] interpreted the Devonian part of the Beacon Supergroup as a passive margin sequence and the Upper Carboniferous–Triassic sedimentary sequence as being deposited in a large foreland basin that bordered the East Antarctic craton. Except for pockets of Cenozoic glacial till, there are no sediments younger than the Jurassic within the TAM.

2.3. Kukri Peneplain

The Kukri peneplain which is extensively exposed along the TAM, is an excellent marker for the preuplift topography of the area because the overlying Beacon Supergroup was hardly deformed after deposition. Near the TAM front, the Kukri peneplain had to be at a depth of ~2.7–3.5 km at the end of Beacon Supergroup deposition to accommodate the deposition of fluvial and shallow marine deposits. It is now found at elevations of 500–4000 m above sea level, and its presence in these elevations indicates the extent of rock uplift.

2.4. Ferrar Flood Basalts

The Ferrar Supergroup is a thick sequence of sills, basalt flows, and pyroclastic rocks of tholeiitic composition mostly dated at about 177 ± 2 Ma [*Heimann et al.*, 1995]. Dolerite sills and dikes are exposed throughout the Transantarctic Mountains, emplaced mainly into the Devonian to Jurassic Beacon Supergroup and only locally into pre-Devonian basement (Figure 2). Individual sills are up to 400 m thick [*Elliot*, 1992]. Although the Ferrar dolerites are considered to be part of a wider-spread Gondwana magmatism (including the Karoo flood basalts), the Ferrar province reflects melting of more depleted lithospheric mantle than basalts of the same age elsewhere in Gondwana [*Elliot*, 1992].

2.5. Timing of Uplift of the TAM

Apatite fission track dating indicates rock uplift of up to 7–8 km in places since the early Cenozoic (55 Ma) [*Fitzgerald*, 1992, 1994]. The rate of uplift though has not been resolved: Several lines of evidence suggest that high relief already existed in the late Oligocene [*Barrett et al.*, 1989] and that Plio-Pleistocene uplift was small (~200 m [*Clapperton and Sugden*, 1990], but *Behrendt and Cooper* [1991] argue that the relief is young (<3 Ma).

2.6. Wilkes Subglacial Basin

Most geological inferences about the Wilkes Basin are based on geophysical data because the basin is covered by up to 3 km of ice. *Drewry* [1976] and *Steed* [1983] interpreted the negative gravity anomaly in conjunction with a negative magnetic anomaly over the basin to indicate the presence of a 2- to 3-km-thick relatively low-density sedimentary layer that fills depressions in a rifted continental crust. *Stern and ten Brink* [1989] and *ten Brink and Stern* [1992, Figure 8] argued against this interpretation because a rifted basin of such great width must be locally compensated, and therefore the gravity effect at the center of the basin should approach zero. They proposed a flexural origin for the basin, and their model implies a shallow (a few hundred meters) depression. *ten Brink and Stern* [1992] further suggested that some vertical movements in the interior of other continents (e.g., the Nile valley behind the Red Sea hills, the Kalahari Basin behind the Great Escarpment of southern Africa) are, in fact, the result of regional isostasy in which uplift of the rift flank has created a broad subsidence in the interior of the crustal block. This association is often overlooked because of the large distance between uplift and subsidence, which is a function of the high flexural rigidity of the lithosphere.

3. Data Acquisition

The East Antarctic Seismic Traverse (EAST93) started 25 km west of the westernmost outcrop in the area, Lashly Mountain (Figure 3a), and 10 km west of the Taylor Dome ice drill site [*Waddington et al.*, 1994]. It extended subparallel to latitude 78°S, ending over the Wilkes Basin, 323 km west of the

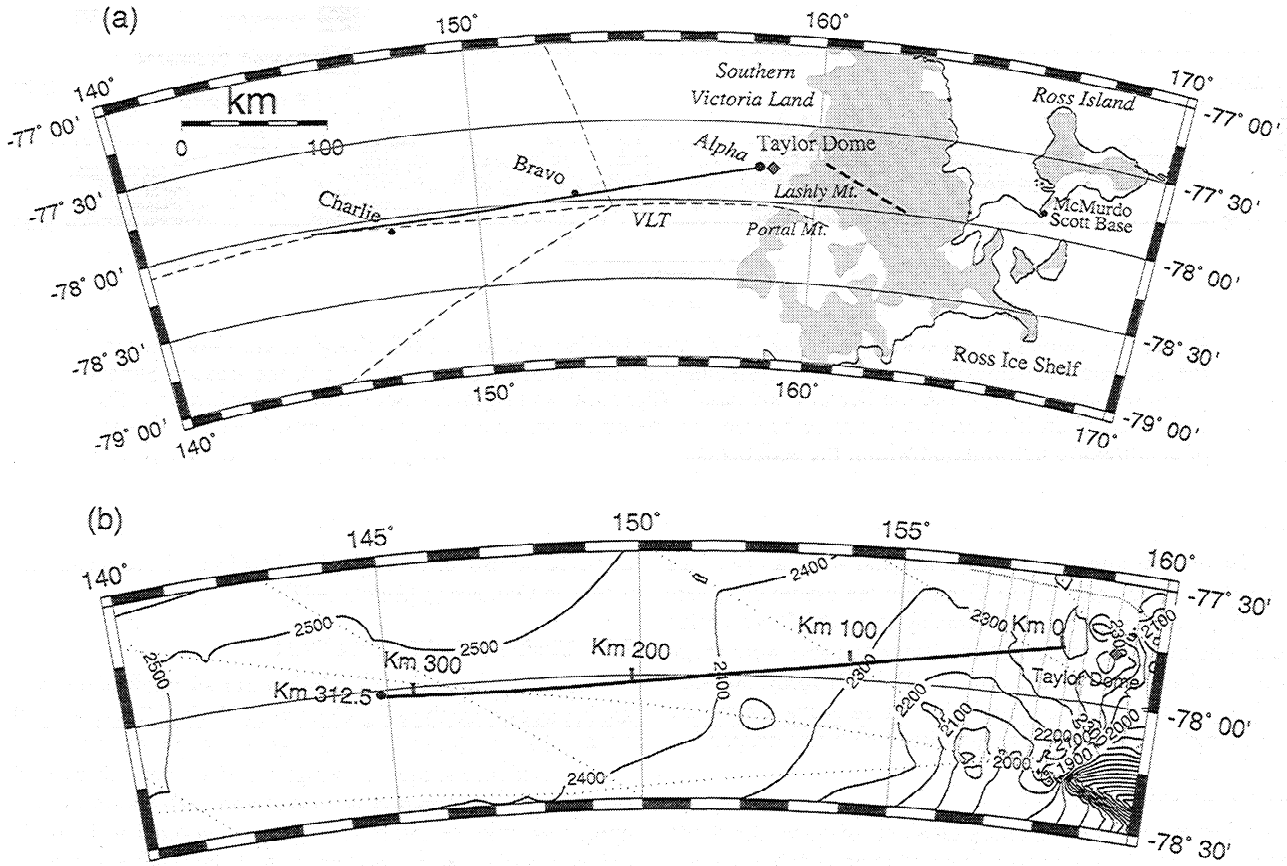

Figure 3. Detailed maps of the region surrounding EAST93. Heavy line is route of EAST93 traverse. (a) Traverse route in relation to the route of the Victoria Land Traverse (VLT) 1958–1959 [*Crary*, 1963]. Taylor Dome, 10 km east of the start of our traverse at point Alpha, is the location of an ice core which reached bedrock at 554 m below the surface [*Waddington et al.*, 1994]. Absolute elevation was measured at points Alpha, Bravo, and Charlie as part of the survey. Heavy dashed line is location of geological cross section in Figure 2. (b) Surface elevation of the ice sheet from airborne radar data collected during the 1970s [*Drewry*, 1982, 1983]. Dotted lines are airborne radar tracks [*Drewry*, 1983].

drill site. Data collected along the traverse included 236 km of high-resolution multichannel seismic reflection data with a 150-m shot interval; 312.5 km of gravity data collected at 2.1-km intervals; 312.5 km of total field intensity magnetic data collected on average at 500-m intervals; and 205 km of ground penetrating radar data at 77-m intervals. Positions and elevations were determined at 150-m intervals along the traverse using optical leveling. This leveling was tied to accurately measured Global Positioning System (GPS) stations at points Alpha, Bravo, Charlie, and Taylor Dome (Figure 3a). The estimated accuracy of this technique was ±1 m for position and ±2 m for elevation [*Hackney*, 1996; *ten Brink and Bannister*, 1995].

Seismic data were acquired with a towed snow streamer. The streamer was towed at a constant distance (175–185 m) behind the shots, which were spaced every 150 m. The 40- to 60-m-long detonating cord with 40–60 g/m of dynamite (total of 1.6–2.4 kg) was used as a sound source. A snow plow laid the cord 16.5 cm below the surface and buried it. Detonating cord was chosen as a source to achieve a high acquisition rate and to avoid drilling shot holes. Nominal common midpoint (CMP) fold was one, but up to 10 traces were binned in 25-m intervals to produce Figure 4. Routine processing was applied to the data.

The seismic signal returned from subglacial layers (Figure 4a) was disappointingly low relative to ambient noise and "ground roll." Bed topography could be clearly seen in the eastern 75 km of the traverse where the ice is relatively thin (700–1700 m) but was faint farther west at depths of 2000–3000 m. It appears that the high near-surface velocity gradient in the ice generates strong turning waves and surface waves at the expense of more deeply penetrating energy. However, this must only be a partial explanation in light of positive test results with detonating cord as a seismic source on the Ross Ice Shelf [*ten Brink et al.*, 1993] and in West Antarctica (S. Anandakrishnan, personal communication, 1995), where surface temperatures are warmer. Prolonged surface noise was reported on the East Antarctic polar plateau during the 1949–1952 Norwegian-British-Swedish Antarctic expedition and the 1957–1961 geophysical traverses, but it was significantly lower at warmer surface temperatures [*Bentley*, 1964]. That noise was attributed to incoherent surface waves whose decay time increases with decreasing temperatures [*Bentley*, 1964]. Alternatively, vertical and lateral heterogeneities in elastic properties near the surface due to alternating hard ice and soft snow may limit wave propagation. Persistent katabatic wind with speeds of 10–40 km/h throughout the experiment has undoubtedly added to the ambient noise.

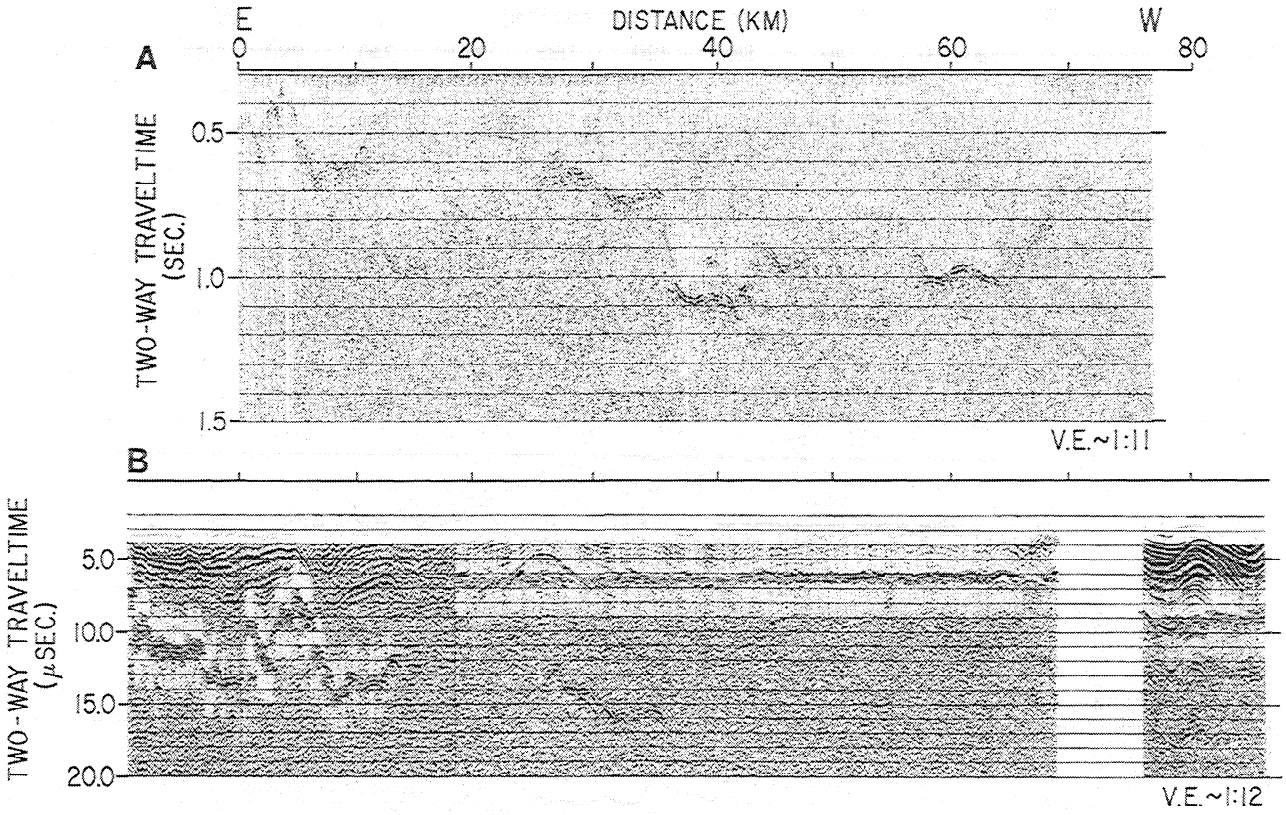

Figure 4. Coincident (a) seismic reflection and (b) ground-penetrating radar profiles between Taylor Dome and km 85 showing the ice bedrock interface along the eastern part of EAST93. Only a few discontinuous reflections can be observed on the seismic line below this interface. Shallow reflections in the radar profile are due to layering and impurities within the ice. The ice is being deformed and folded as it flows over the bed topography. Strong horizontal reflections at 6 and 9 μs in the radar data are artifacts.

An independent image of the bed topography was provided by a ground-penetrating radar system (Figure 4b). The system was towed on sleds and acquired data underway [*ten Brink and Bannister*, 1995]. Measurements were made from Taylor Dome (km −10) to km 195.5, but penetration was limited to 1500 m depth. The system included low-frequency receiving and transmitting antennae (1.25 MHz) with resistivity constants of 400 ohms. The radar transmitter supplied a voltage pulse of 750 V. Data were sampled for 40 μs at 0.08 μs per sample by a digital oscilloscope which stacked 256 readings to form one trace. Data were recorded on a portable computer and later converted into SEG-Y format which allowed the use of standard seismic processing tools for display and analysis (Figure 4b).

Gravity data were collected with a LaCoste and Romberg gravimeter. Apart from a 5.19-mGal adjustment for a "tear" that occurred toward the end of the traverse, a simple linear drift correction of 0.05 mGal/d was applied. The measurements were tied to permanent stations at McMurdo and Scott bases on Ross Island. Magnetic data were collected in the field with two Geometrics G-856 proton precession magnetometers. During any one day of work, one magnetometer was used for measurements at set distance intervals along the traverse, while the other recorded continuously at the temporary camp.

4. Data

Depth to bedrock was determined by picking reflections from the seismic and radar sections and converting the two-way travel times to depth (Figure 5a). The reflectors were first migrated to assure their proper position. Seismic velocity in the Polar Plateau increases with depth, reaching normal ice velocities at 160 m depth, the base of the compacted snow (firn) layer [*Crary*, 1963]. The velocity gradient above 160 m depth was averaged, and a constant P wave velocity of 3880 m/s was assumed for depths below 160 m. This is the average seismic velocity in plateau regions [*Robinson and Splettstoesser*, 1984] and is consistent with ice core velocity measurements from the Taylor Dome drill hole [*Fitzpatrick*, 1994]. An electromagnetic wave velocity in ice of 168 m/μs [*Drewry*, 1982] was used for depth conversion of the radar data. The radar and seismic depths were compared for consistency (inset in Figure 5a). They were also checked against other more detailed radar depth measurements made in the vicinity of Taylor Dome (D. Morse, personal communication, 1996) and against the depth to bedrock at the Taylor Dome drill hole (554 m [*Waddington et al.*, 1994]). Depth estimates from regional and continent-wide airborne radar surveys (Figure 3b) were interpolated along our traverse (Figure 5a). The estimated errors in these airborne surveys were <5 km in navigation, 1% in ice velocity, and 50–150 m in flight height [*Drewry*, 1982, 1983] but were probably larger along our traverse because of the interpolation of sparse track lines. Nevertheless, our depth-converted seismic and radar profiles are consistent with the regional surveys (Figure 5a).

The seismic and radar data show mountainous subglacial

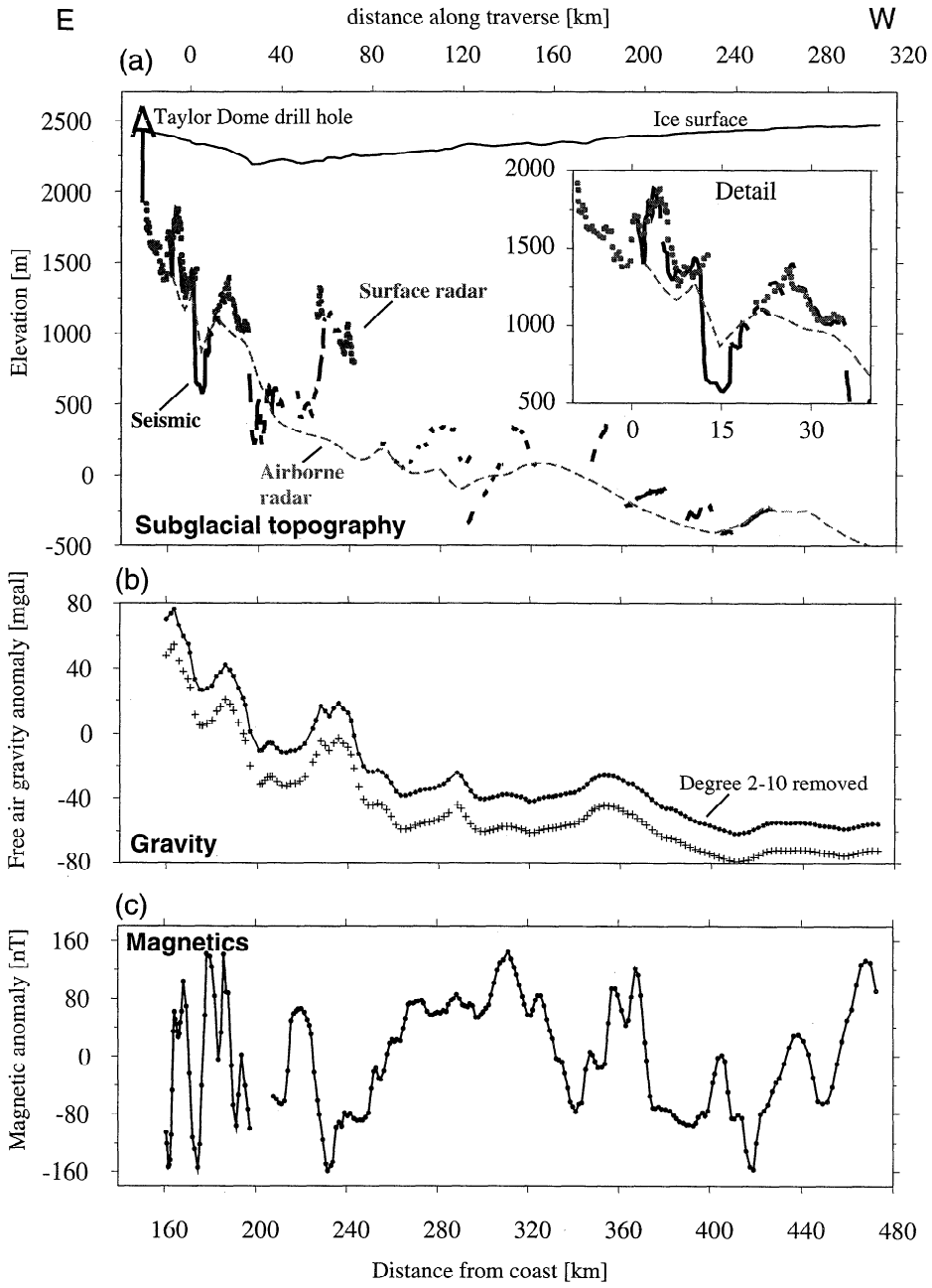

Figure 5. (a) Ice surface and bedrock elevations along the EAST93 traverse. Ice surface elevation was measured every 0.15 km with estimated error of ±1 m. Reflections on the seismic (solid lines) and radar (gray dots) profiles (e.g., Figure 4) were hand migrated and converted to depth. Dashed gray line is extrapolated bedrock surface along EAST93 from gridded airborne radar data collected during the 1970s (D. Vaughan, personal communication, 1993) [*Drewry*, 1983]. Inset shows detailed enlargement of the first 30 km of the traverse. Radar depths were shifted upward by 100 m to match other radar data from Taylor Dome (D. Morse, personal communication, 1996). Discrepancies between the seismic and radar profiles in some places may be due to inaccurate distance measurement by the wheel attached to the radar sledge. (b) Free air anomalies (crosses) and residual free air gravity anomalies (solid line with dots) after subtraction of satellite gravity field summed from degree 2 through 10. (c) Diurnally corrected magnetic anomalies relative to International Geomagnetic Reference Field (IGRF) 1990 after removal of a linear trend.

topography beneath the eastern 85 km. Because the start of the line is about 160 km from the coast, the total width of the TAM in this area appears to be about 245 km. A wide valley at km 30–60 coincides with a surface depression in the ice (Figures 3b and 5a) which separates the Taylor ice dome area from the interior of the plateau. The ice-rock interface beyond km 85 is only intermittently imaged but appears to deepen gradually toward the center of the Wilkes Basin.

Gravity anomalies were calculated using the Geodetic Reference System Formula of 1967. The elevations used for the free-air correction were referenced to the geoid, which is −50 m lower than the spheroid in this region. The free-air anomaly

is accurate to ±1 mGal [*Hackney*, 1996] because of the accurate elevation determination. We further subtracted the satellite gravity field components of degrees 2 to 10 (C. Bowin, personal communication, 1996), the source of which is believed to reside in the lower mantle [*Bowin*, 1991]. These components amount to 16–21 mGal and are almost uniform along the line (Figure 5c). The residual gravity anomaly mimics the variations in topographic elevations and ruggedness.

Magnetic data were reduced as follows: corrections to the diurnal variation of the magnetic field were made using the record of the permanent magnetic observatory at Scott Base. The Scott Base record was used, despite its large distance (150–500 km) from our traverse [*Hackney*, 1996], because of the good correlation between the Scott Base record and the data recorded by the field base station. After correction for diurnal variations, several spurious "jumps" remained in the data. Where the bedrock is deep (>2 km), these jumps were removed by applying an 8.5-km spatial filter to the data [*Hackney*, 1996]. Magnetic anomalies (Figure 5c) were calculated by subtracting the reference field during the experiment (International Geomagnetic Reference Field (IGRF) 1990 [*Langel*, 1992] and a linear trend. Anomalies with amplitude of up to 250 nT are present along the entire profile. Steep magnetic gradients are observed at km 75, roughly at the western edge of the mountainous topography and at km 210 and 290 despite the great depth to bedrock there.

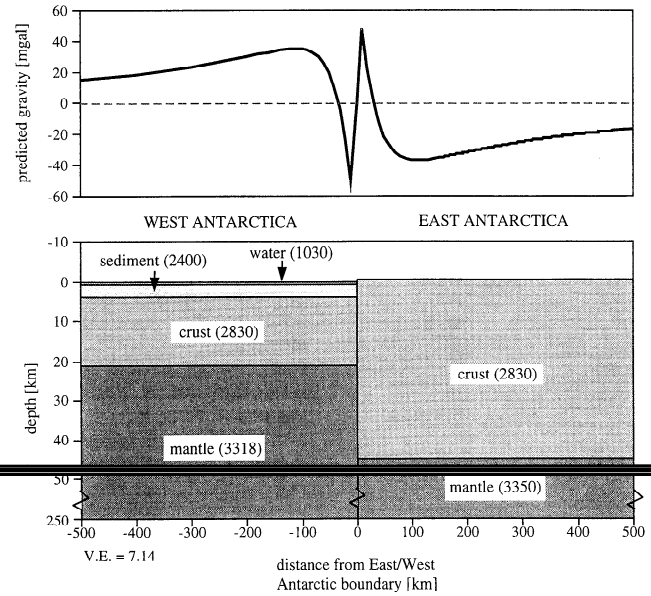

Figure 6. An isostatically balanced crustal model for East and West Antarctica above a 250-km compensation depth, showing the gravity edge effect and the long-wavelength negative anomaly over East Antarctica that result from the juxtaposition of two contrasting lithospheric regions. Values shown in parentheses are density in kg/m^3. This configuration is modified by applications of the loads in Figure 7 to produce the flexural uplift of the TAM in Figure 9a.

5. Modeling Procedure

The results of the EAST93 geophysical traverse provide for the first time coincident detailed data sets of bed topography and gravity to test the flexural models for the uplift of the Transantarctic Mountains.

5.1. Starting Model

There are many possible density structures that can explain any given gravity data set. This nonuniqueness can be partly countered by applying constraints from other data, such as magnetic and seismic. However, before such constraints are applied, the nonuniqueness of predicted structures can also be reduced by considering only density structures that maintain mechanical equilibrium with some reasonable Earth structure [e.g., *Lyon-Caen and Molnar*, 1989]. The initial model used here is one in which isostatic equilibrium is maintained between East and West Antarctica (Figure 6).

The average structure of the West Antarctic region of the model consists of a 700-m water column overlying a 4-km-thick layer of rift-related sediments. The Moho is at an average depth of 21 km [*ANTOSTRAT Project*, 1995; A. Cooper, personal communication, 1996]. The East Antarctica crustal column is chosen to be in equilibrium with the global average continental crust thickness, 41.5 km, and density (2830 kg/m^3) [*Christensen and Mooney*, 1995] for lack of better constraints. The elevation range of East Antarctica prior to the uplift of the TAM is estimated from fission track and landform evolution analyses to have been between 500 and 1100 m [*Fitzgerald*, 1992; *Sugden et al.*, 1995]. For East Antarctica to remain in isostatic equilibrium while having an "average" crust, such a range of elevations requires a crustal thickness between 44.1 and 47.9 km, in agreement with previous estimates for East Antarctica [*Bentley*, 1991; *Roult et al.*, 1994].

In order to maintain isostatic equilibrium between East and West Antarctica, the density of lithospheric mantle underlying West Antarctica should be less than that under East Antarctica. The density contrast depends on the compensation depth. We chose a compensation depth of 250 km, corresponding to a lithospheric root under cratons. The average upper mantle density under West Antarctica is 3318 kg/m^3, 32 kg/m^3 or approximately 1% less than under East Antarctica, and in agreement with estimates based on geotherms of these two regions (see below). The juxtaposition of two contrasting lithospheric regions is responsible for two effects in the gravity field, a short-wavelength "edge effect" and a broad gravity low that extends several hundred kilometers into East Antarctica (Figure 6). Gravity edge effects are observed across many lithospheric boundaries including that between East and West Antarctica [*Stern and ten Brink*, 1989, Figure 12]. The broad low is the result of low-density mantle under West Antarctica.

5.2. Flexure

We next assume, following *Stern and ten Brink* [1989], that uplift of the TAM is supported by a broad flexure or bending of the strong East Antarctic lithosphere. Lithospheric flexure in response to large (tens to hundreds of kilometers) long-term (>10^5 years) loads such as volcanoes, sedimentary basins, and thrust faults can be modeled to a first approximation, as the bending of a thin elastic plate that overlies a fluid substratum. The resistance to bending, or the stiffness of the plate, is described by its flexural rigidity D, a parameter which empirically depends on the temperature gradient and the composition of the plate and is proportional to the thickness of the elastic plate, T_e (Table 1). The vertical deflection $w(x)$ of a thin elastic plate in two dimensions is given by

$$Dd^4w/dx^4 + \Delta\rho g w = P \qquad (1)$$

Table 1. Parameters Used in This Study

Parameter	Value	Description
D	$ET_e^3/12(1 - \sigma^2)$	flexural rigidity
α^4	$4D/g\Delta\rho$	flexural parameter
E	8×10^{10} Pa	Young's modulus
σ	0.25	Poissons' ratio
g	9.8 m s^{-2}	gravitational acceleration
$\Delta\rho$		density difference between materials overlying and underlying the plate
ρ_m	3350 kg/m^3	upper mantle density under East Antarctica
ρ_c	2830 kg/m^3	global average crustal density [*Christensen and Mooney*, 1995]
ρ_s	2400 kg/m^3	sediment density
ρ_w	1030 kg/m^3	water density
ρ_i	920 kg/m^3	ice density
α	3.4×10^{-5} K^{-1}	coefficient of thermal expansion
k	3.2 W m^{-1} K^{-1}	conductivity of the lithosphere
κ	1×10^{-6} m^2 s^{-1}	thermal diffusivity
T_0	1330°C	asthenospheric temperature
A	$A_0 \exp(-z/D)$	radioactive heat production within the crust
A_0	1.7 μW/m^3	radioactive heat production at the surface
D	1/4 crustal thickness	depth in which radioactive heat production decays to $1/e$
T_{grad}	44.7°C/km	Surface temperature gradient from measured heat flow in the Ross Sea of 71 mW/m^2 [*Blackman et al.*, 1987] and sediment conductivity of 1.6 W/m K

(i.e., bending resistance plus buoyancy forces equals load), where P is the load that drives the deformation. Equation (1) is solved numerically using a finite difference routine (modified from *Bodine et al.* [1981]) which allows for lateral variations in flexural rigidity, load distribution, and restoring force in the manner shown in Figure 7. We assume that the East Antarctic lithosphere has a free edge at the TAM front, $x = 0$, and thus acts as a semi-infinite or a broken plate. The boundary conditions at the break are zero moments and shear stresses, i.e., $d^2w/dx^2 = 0$; $d^3w/dx^3 = 0$; and at $x = \infty$, the boundary conditions are zero vertical displacement and slope, i.e., $w = 0$; $dw/dx = 0$.

We apply the semi-infinite elastic plate model to the configuration shown in Figure 6 in order to flex the margin of East Antarctica and to produce the geometry of the TAM and the Wilkes Basin. We consider the following loads: thermal buoyancy, rebound due to erosion, the load of the ice sheet, and an additional end load (Figure 7), and we apply these loads to models with a variety of flexural rigidities. Thermal buoyancy and the rebound to erosion can by themselves account for almost all the observed rock uplift. Their amplitude and lateral distribution can be estimated using certain assumptions as outlined below. The load of the ice sheet is the only load which is directly observed. Rock uplift due to the load of the ice sheet is insignificant (100–200 m, see *Stern and ten Brink* [1989] for discussion), but its lateral distribution modifies somewhat the flexural profile inland of the TAM. The end load is a point load applied to the edge of the plate, which was added to keep the amplitude of rock uplift at the edge of the TAM fixed to 7.2 km (see section 5.2.2) for all flexural rigidities and is therefore variable in magnitude. This point load is small, <10% of the total upward force required to lift the TAM, and may not be necessary should a more accurate estimate of thermal buoyancy and erosion be developed. Alternatively, it can be interpreted to represent a mechanical rebound to the unloading by the Ross Embayment [*Stern and ten Brink*, 1989] or the result of bending moment due to thermal stresses in the East Antarctic lithosphere.

5.2.1. Thermal buoyancy load. A geotherm for East Antarctica (Figure 8) is calculated using a 250-km-thick cooling plate model with a thermal age of 530 Ma, which corresponds to the latest orogeny in the TAM, the Ross Orogeny, and an exponential radiogenic heat production with depth in the crust. A geotherm for the Ross Embayment is calculated assuming a 125-km-thick cooling plate with a thermal age of 70 Ma (i.e., the geotherm of Ross Embayment was not set to zero-age crust at the end of the main extension phase) and the parameters given in Table 1. In the absence of other constraints about the thermal history of both the Ross Embayment and the TAM, we simplify the calculation by assuming that both geotherms were kept in steady state since 70 Ma, while the TAM and the Ross Embayment were juxtaposed; that is, we calculate the temperature increase across the edge of East Antarctica (Figure 8) using a one-dimensional (1-D) lateral heat conduction equation for a semi-infinite solid and a constant initial temperature [*Carslaw and Jaeger*, 1959, p. 60]. The geotherm at the TAM front over that time period essentially becomes similar to the Ross Embayment geotherm, which translates to an average temperature increase of 285°C in the 205-km-thick lithospheric mantle. The density reduction due to this temperature increase is 33 kg/m^3. This density reduction is similar to that obtained earlier from isostatic considerations (Figure 6). The distributed uplift force at the TAM front due to thermal buoyancy integrated over the 250-km-thick lithosphere is 8×10^7 N/m^2. Farther inland the force decreases as temperatures decrease. We approximate this decrease in the model by preserving the density reduction and decreasing the height of the buoyant column (Figure 7d).

5.2.2. Erosion. Elevated topography of different ages is maintained well beyond the time at which the thermal processes associated with extension have died out because erosion of the uplifted terrain causes unloading which in turn induces isostatic rebound of the lithosphere [*Weissel and Karner*, 1989]. Erosional unloading will not cause a significant rock uplift of the TAM on its own even if East Antarctica were at elevation of 500–1100 m prior to the initiation of uplift [*ten Brink and Stern*, 1992], but once uplift is initiated, its contribution is important. For the TAM, the amount of material removed by erosion is the difference between the amount of rock uplift and the current topographic profile. The TAM contain no strata with ages that span the time of the most recent uplift, and hence other means must be employed to determine the

amount of uplift. Data points from an apatite fission track uplift profile for southern Victoria Land [*Fitzgerald*, 1992] were extrapolated to the coast, where the amount of rock uplift can be approximated as 7.2 km. The amount of material eroded (Figure 7c) is the difference between the apatite fission track profile and some approximation to the current topography of the TAM.

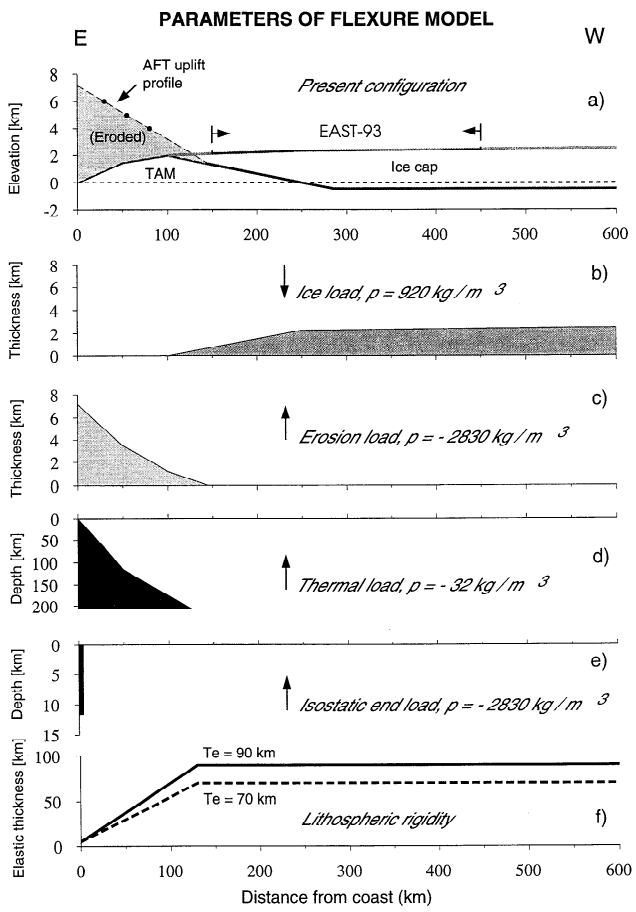

Figure 7. Details of loads and the distribution of elastic thickness applied to the margin of the East Antarctic crust in order to flexurally uplift the TAM. (a) Simplified present geometry used to estimate the loads. Heavy dots are estimated rock uplift from apatite fission track (AFT) analysis [*Fitzgerald*, 1992]. The shaded region between the AFT profile and the approximation to present topography represents the eroded material, shown in Figure 7c. (b) The load of ice above sea level. The remainder of the ice is incorporated in the restoring force component in the finite difference flexural routine. The ice load depresses the Wilkes Basin by ~800 m and shifts the point of minimum elevation farther away from the TAM, but its effect on the magnitude of uplift is minimal. (c) Erosion load, i.e., the difference between the AFT uplift profile and an approximation to the current topography in the TAM. Crustal rock density is used for the eroded material. (d) Thermal load resulting from lateral heat conduction from the mantle lithosphere of West Antarctica into the margin of East Antarctica. (e) Isostatic end load required to match the 7.2 km of uplift at the coast as extrapolated from AFT data in South Victoria Land. (f) Variation of elastic thickness (T_e) toward the interior of East Antarctica. Models with a T_e range of 20–150 km were tested, but only examples with T_e = 70 and 90 km are shown. A reduction in elastic thickness from its average value 130 km inland from the coast to T_e = 5 km at the coast is common to all the models.

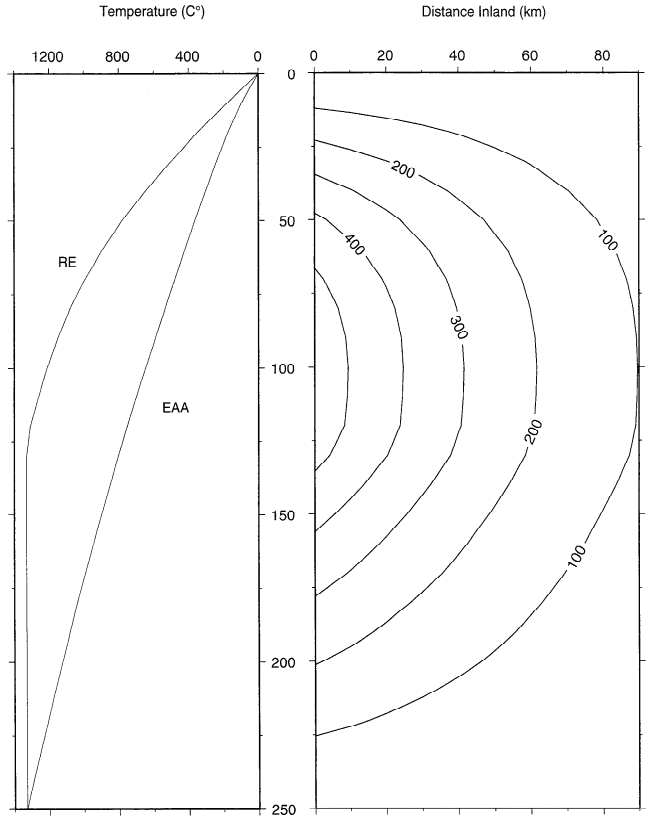

Figure 8. (left) Calculated geotherms for East Antarctica (EAA) and the Ross Embayment (RE) (right) Contours of increased temperatures within the East Antarctic lithosphere as a function of distance from its boundary with the Ross Embayment. The average temperature increase over the thickness of the lithosphere was used to calculate the thermal buoyancy load in Figure 7d.

5.2.3. Flexural rigidity. In order to determine which elastic model of East Antarctica best matches the data from EAST93 and other constraints from the TAM, we applied the loads discussed above and shown in Figure 7 to plates with elastic thicknesses ranging from T_e = 20 to 150 km. In Figure 7f, examples of the lateral elastic thickness variation are shown for models with T_e = 70 and 90 km. In all the tested models, T_e was reduced toward the free edge of the elastic plate. *Stern and ten Brink* [1989] also found that such a variation was necessary to match the observed dip of the Kukri peneplain and argued that this variation in T_e is not unreasonable given the likely physical properties toward the edge of East Antarctica. They argued that T_e would be reduced by the high curvature of the plate at its edge, leading to near-surface elastic failure and ductile flow at depth. Additional reduction in T_e arises from the thermal weakening resulting from the heat transfer from the West Antarctic lithosphere. Additional evidence for a weak edge will be presented in section 7.

6. Elastic Thickness and Preuplift Elevation of East Antarctica

The loads discussed above were applied to the configuration shown in Figure 6 for a range of elastic thicknesses between 20

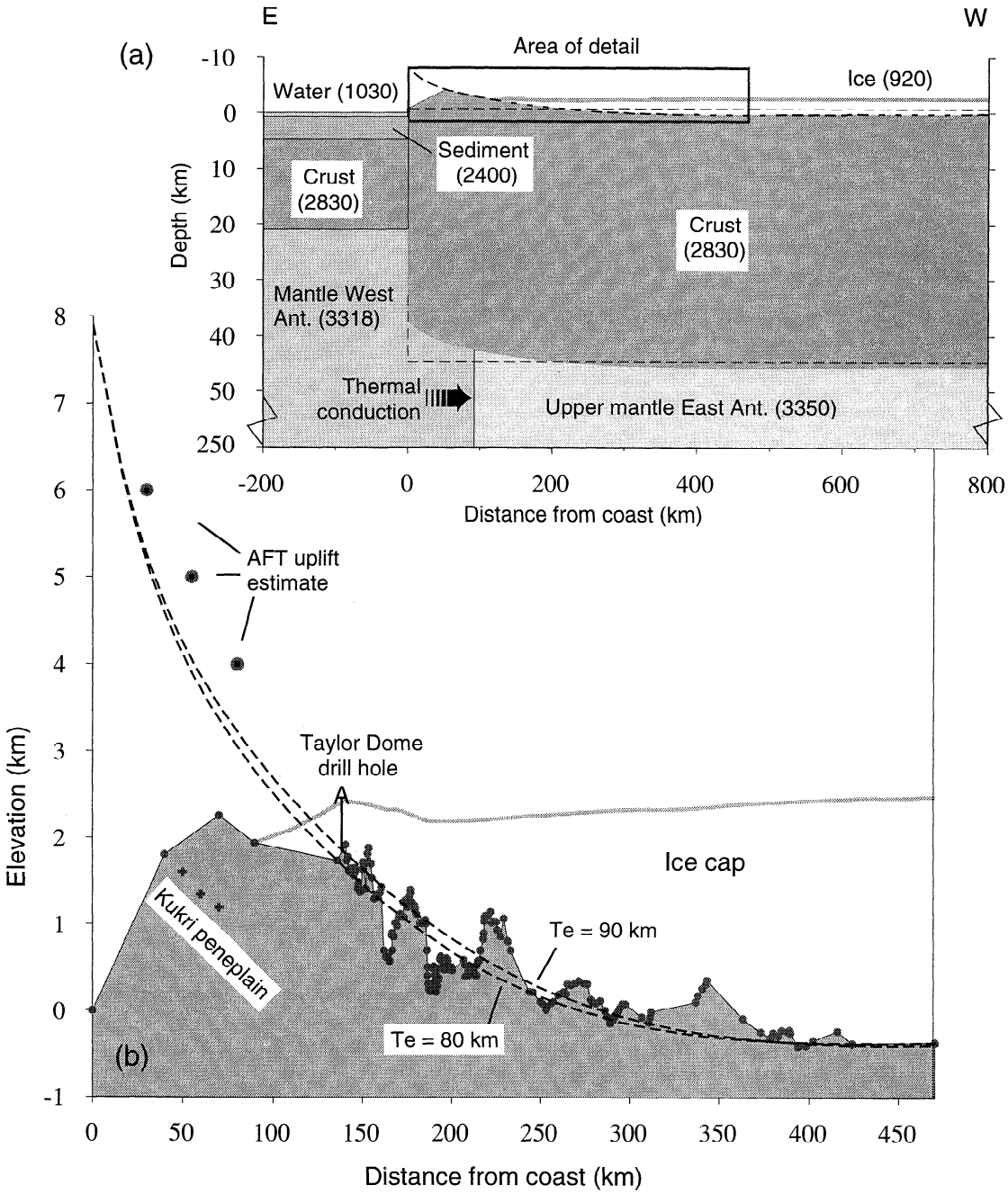

Figure 9. Results of flexural modeling. (a) Flexural uplift of the TAM after loading the edge of East Antarctica in Figure 6 with the loads and elastic thickness distribution of Figure 7. Dashed lines are flexure of the upper and lower (Moho) boundaries of the crust and preflexure crustal configuration. Densities are in kg/m^3. A region of reduced density, providing the thermal uplift force, is shown extending under the TAM. The heavy box outlines the region detailed in Figure 9b. (b) Flexural profiles (dashed lines) superimposed on bed topography along EAST93. The profiles shown are for two different elastic thicknesses, T_e = 80 km and T_e = 90 km and a preuplift reference elevation of 700 m. Ice surface and bedrock elevations (dots) are from Figure 5. Uplift at the coast is 7.2 km (see Figure 7) plus preuplift reference elevation. Other constraints include depth to bedrock at the Taylor Dome drill site [*Waddington et al.*, 1994], the dip of the Kukri peneplain within the TAM [*Stern and ten Brink*, 1989], and uplift estimates from apatite fission track (AFT) analysis in southern Victoria Land (heavy dots [*Fitzgerald*, 1992]).

and 150 km and resulted in the bending of the margin of East Antarctica to produce the TAM (Figure 9a). The modeled topography and gravity profiles were compared with the observed bed topography and gravity profiles to determine the elastic thickness of the best fitting model.

The flexure routine used to compute flexure profiles does so with respect to an arbitrary reference elevation. For each of the elastic thicknesses used, we assume a reference elevation in the range 500 to 1100 m consistent with the elevation of the East Antarctic plateau prior to the TAM uplift [*Fitzgerald*, 1992;

Sugden et al., 1995]. We compare the resulting profiles from the range of elastic thicknesses and reference elevations with the bed topography determined from EAST93 data. Two example flexure profiles with T_e = 80 and 90 km and a preflexural elevation of 700 m are plotted over the bed topography in Figure 9b. The bed topography is obtained from the interpretation of seismic and radar sections shown in Figure 5a. Preference has been given to seismic reflections, and radar data have been used to fill gaps where there are no seismic reflections. Straight lines are drawn between points where neither seismic nor radar reflections are observed.

The fit between flexure and bed profiles is quantified by computing the root-mean-square (rms) error of the fit between the two profiles. Those rms errors are contoured and plotted in Figure 10 (solid contours). The trough of lowest rms error is bounded by T_e in the range 60 to 80 km and preflexural elevations of 700 to 900 m. On this basis, the EAST93 data indicate that the elevation of East Antarctica prior to flexure and uplift of the TAM was 800 ± 100 m and its elastic thickness was 70 ± 10 km. However, the topographic surface to which flexure profiles have been fit has undoubtedly been modified by erosional processes.

To avoid uncertainty arising from erosion, the matching of observed gravity anomalies to those calculated from a range of possible models is more appropriate. Such an approach will include the integrated effects of mass distribution throughout the entire lithosphere. Free air anomalies were computed from flexure models with densities specified in Figure 9a for a range of elastic thicknesses and reference elevations. The rms misfit differences between the calculated anomalies and the EAST93 free air anomalies (Figure 5b) were computed (dashed contours in Figure 10). Model parameters which best fit the observed gravity anomaly are T_e = 85 ± 15 km and a preflexural elevation of 700 ± 50 m. These parameters were chosen as our best estimates. It is reassuring that the best fit values derived from gravity overlap those derived from the bed topography. Our estimate of elastic thickness is less than the estimate of *Stern and ten Brink* [1989], which was based on a stack of five topographic profiles, and greater than the estimate of *van der Beek et al.* [1994], which was based on sparse gravity and did not consider either the topography nor the gravity fields of the Wilkes Basin region. An elastic thickness of 85 ± 15 km indicates a flexural rigidity between 2.4×10^{24} and 7.1×10^{24} N m for East Antarctica away from its margin with West Antarctica. This high rigidity is typical of old cratonic regions (10^{24}–10^{25} N m) such as Western Australia [*Zuber et al.*, 1989] and southern Africa [*ten Brink and Stern*, 1992] and is higher by 2 orders of magnitude or more than the rigidity of rifts and continental margins. The thermal lithosphere of East Antarctica is indeed expected to be thick as we assumed in calculating the geotherms earlier because the flexural rigidity is strongly dependent on the thermal gradient of the lithosphere.

The flexural profile from which the elastic thickness is derived depends on the spatial distribution of the loads. An analytical solution to equation (1) for a broken elastic plate with a load applied at the edge, $x = 0$, and a constant flexural rigidity D [*Walcott*, 1970] is

$$w(x) = (2P\alpha/g\Delta\rho)e^{-x/\alpha} \cos (x/\alpha) \qquad (2)$$

The distance from the axis of maximum uplift to the minimum bedrock elevation of Wilkes Basin (also known as the flexural half wavelength) is given by

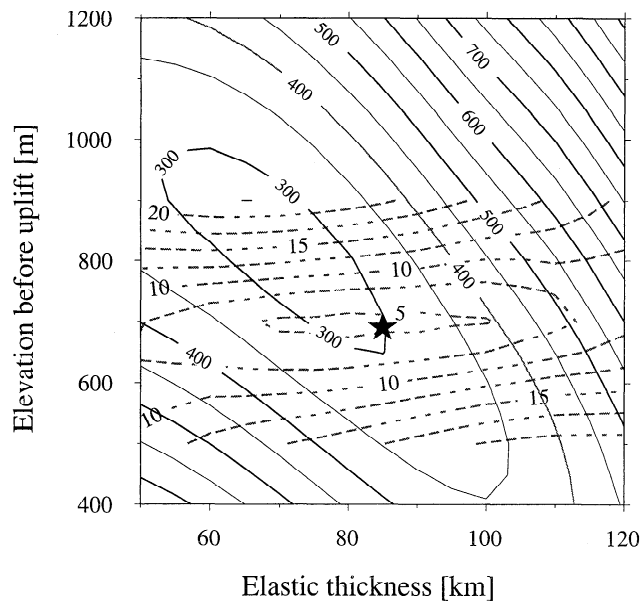

Figure 10. Contours of root-mean-square (rms) differences between flexural models with various combinations of elastic thickness (T_e) and preuplift elevation to observed data. Solid contours are rms differences between the bed topography and the flexure profiles (contour interval is 50 m). Dashed contours are rms differences between the observed free air anomalies (Figure 5c) and free air anomalies calculated from the flexural models (contour interval is 2.5 mGal). Density for different parts of flexural models is given in Figure 9a. Star is our preferred elastic thickness and preuplift elevation for East Antarctica from the combined fit.

$$x = 0.75\pi\alpha \qquad (3)$$

In East Antarctica this distance is 450 km, which yields an elastic thickness of 105 km. However, with the thermal and erosion loads extending 130 km inland and with the ice increasing in thickness to a distance of 250 km, the flexural half wavelength is larger than in the analytical solution. A corollary conclusion of this modeling is therefore that although the load of the ice sheet has little influence on the magnitude of uplift of the TAM [*Stern and ten Brink*, 1989], the ice load modifies the distance to the lowest point in the Wilkes basin. *ten Brink and Stern* [1992, Figure 13] discussed a similar example in which loading in the hinterland increases the apparent flexural half wavelength. They showed that the lowest point in the southern African interior, 900 km from the coast, can be fit with an elastic plate model with T_e = 100–120 km if erosion and redeposition took place in the hinterland as a result of the uplift.

7. Discussion: Uplift as a "Transform-Flank" Phenomenon

The TAM uplift has been used together with the Red Sea shoulder uplift as a type example for modeling of rift-flank uplift phenomena [e.g., *van der Beek et al.*, 1994]. In this section we bring a variety of evidence to show that the uplift is spatially and temporally decoupled from the rifting between East and West Antarctica. We suggest that transtensional motion may have broken the elastic plate which was already loaded by thermal buoyancy of the mantle lithosphere following the ex-

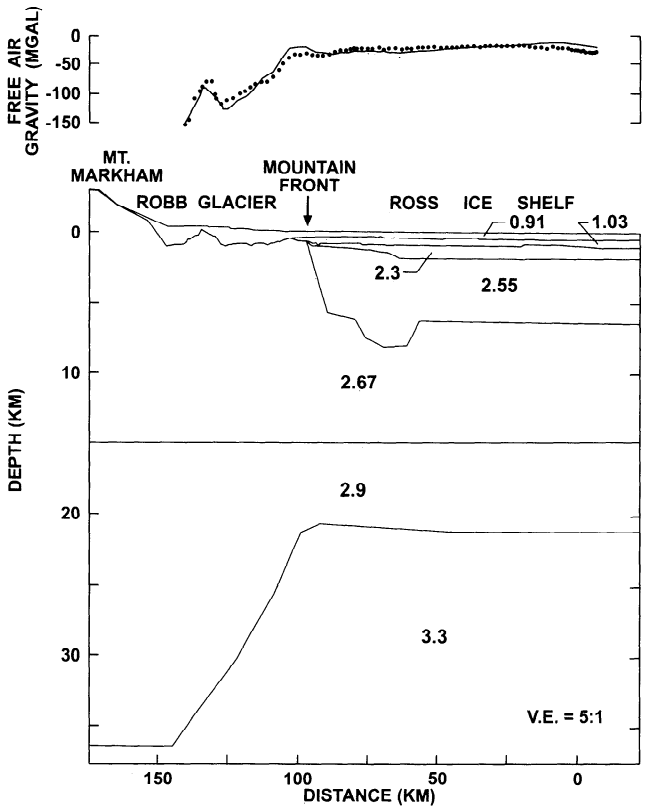

Figure 11. Observed free air gravity anomaly (dots) measured at 2-km intervals along the SERIS seismic profile (see Figure 1 for location) and calculated gravity anomaly (heavy line) from a 2-D density-depth model. The model is based on coincident seismic reflection and refraction data (reprinted with permission from *ten Brink et al.* [1993], copyright 1993 American Association for the Advancement of Science).

tension. This break in the plate, we suggest, has led to rapid uplift, erosion, and exhumation.

7.1. Evidence for a Decoupled Transtensional System

1. Mechanical models for rift-flank uplift predict uplift to develop next to a rifted half graben which is flexed down toward the flank. Such spatial association along the TAM is limited to the 300-km-long Terror Rift (Figure 1), the only section adjacent to the mountains where a deep basin is currently documented. Furthermore, the Terror Rift is considered by some to be a pull-apart or a transtensional basin [*Tessensohn*, 1994], not an extensional basin, and is indeed bound by subvertical faults and upward diverging and rejoining splay patterns [*Cooper et al.*, 1991] which are typical of strike-slip faults. Coincident seismic reflection, refraction, and gravity profiles perpendicular to the TAM front in the central Transantarctic Mountains show no evidence of a Cenozoic rift basin adjacent to the mountains (Figure 11) [*ten Brink et al.*, 1993]. This is despite the fact that rock uplift there is among the highest along the TAM.

2. Ross Island (Figures 1 and 3a) and the adjacent late Cenozoic volcanic edifices (collectively known as Ross Archipelago) are located on the boundary between West Antarctica and the TAM (Figure 12). If the lithosphere of Ross Embayment is coupled with that of the TAM, we expect the volcanic load of the Archipelago to depress the TAM front and with it the relatively flat preuplift marker of the Kukri peneplain. Figure 12 shows, however, that the peneplain near the volcanic load is in places 500–1500 m higher than the elevation of the peneplain away from the volcanic load, not lower as expected if the volcanic load depressed the TAM front. Hence this section of the TAM front does not appear to be influenced by loads in the Ross Embayment. A weak boundary at the TAM front in that area is also indicated by the high crustal temperatures. Thermometric and barometric analysis of granulite inclusions in xenoliths from the area indicate temperatures of 900–1000°C at 25 km depth [*Berg et al.*, 1989]. Olivine at these temperatures deforms ductily at geological strain rates, and the interpolated depth to the 450°C isotherm, a depth often equated with the elastic thickness, is only 6 km.

3. Moho dips steeply (15°–20°) under the mountain front at the central TAM (Figure 11) and at the northern end of the Terror Rift [*O'Connell and Stepp*, 1993], indicating a narrow transition zone between the TAM and the extended crust of the Ross Embayment. Moho dips of similar magnitude are common across transform plate boundaries [e.g., *Spence and Asudeh*, 1993; *Todd et al.*, 1988].

4. The most significant uplift phase of the TAM was initiated at 55 Ma [*Fitzgerald*, 1992, 1994], at least 30 Myr after the cessation of the Late Cretaceous (105–84 Ma) continental extension between New Zealand and West Antarctica [*Lawver et al.*, 1992]. The continental extension formed a vast area of thin continental crust (20–25 km thick) with submerged basins and ridges in the Ross Embayment (Antarctica), the Chatham Rise, and the Campbell Plateau (New Zealand) [*Anderton*, 1982; *ANTOSTRAT Project*, 1995]. The extension ended with the initiation of seafloor spreading between New Zealand and West Antarctica.

5. The initiation of uplift appears, on the other hand, to be coeval with major plate reorganization in the South Pacific, including possible transtensional motion between East and West Antarctica: A major plate reorganization, producing new fracture zones, is recorded in the seafloor between the Campbell Plateau and the Ross Sea between Chrons 27 and 24 (61–53 Ma [*Cande et al.*, 1995]). A dramatic change in rate and spreading directions between 42 and 33 Ma is recorded at the Emerald Fracture Zone (FZ) north of the East-West Antarctic boundary (Figure 1) [*Cande et al.*, 1995]. This plate reorganization was caused by the cessation of spreading in the Tasman Sea, the increase in spreading rate between Australia and Antarctica, and the development of plate boundary through New Zealand. Because these events did not occur simultaneously, the reorganization during this period possibly generated minor movements between East and West Antarctica. *Molnar et al.* [1975] postulated a 500-km relative motion between East and West Antarctica in the early Tertiary and a triple junction between Pacific-Australia and East and West Antarctica at 45 Ma. S. Cande (personal communications, 1994, 1996) attributed a misfit of Eocene age magnetic anomalies along the Southeast Indian Ridge (SEIR) east of Balleny FZ [*Royer and Sandwell*, 1989] to dextral transtensional movement between East and West Antarctica of about 100 km at this time. Recent plate motion reconstruction by *Sutherland* [1995] predicts dextral movement between West and East Antarctica starting at 45 Ma.

6. Fault planes and striae orientations in the TAM, which are interpreted to be of Cenozoic age, suggest a dextral transtensional motion along the Transantarctic Mountain front [*Wilson*, 1995].

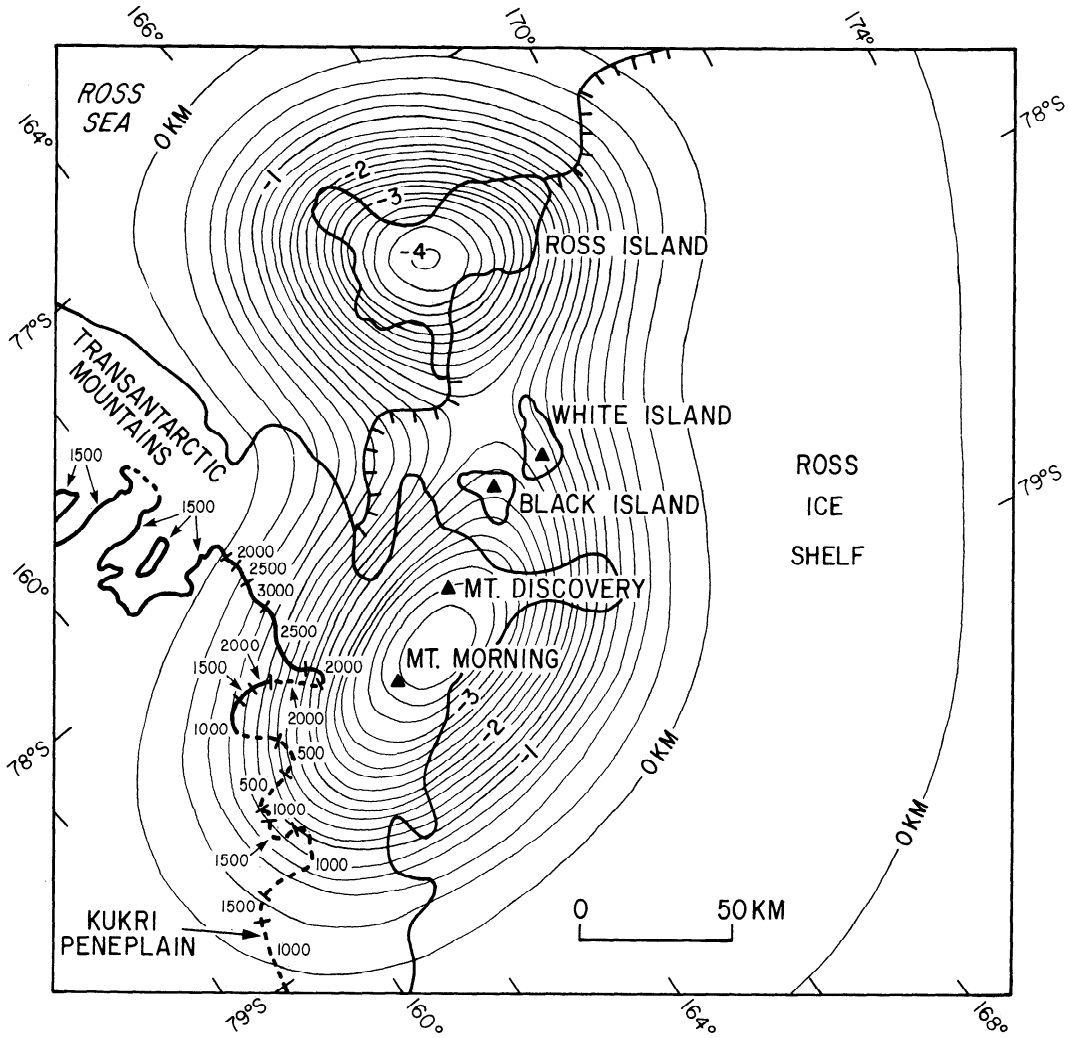

Figure 12. Deflection of the lithosphere (in km) due to the load of Ross Archipelago (see Figure 3 for location) calculated by a 3-D flexure model in the wave number domain (modified from unpublished programs by J. C. Cochran and W. H. Smith). The load comprises the volcanoes shown by solid triangles and Ross Island. The elevation (in m) of the Kukri peneplain, where it intersects the surface [*Warren*, 1969] is overlain in continuous (where certain) and dashed line (where uncertain). This figure was calculated with an elastic plate thickness (T_e) of 5 km. Models with larger T_e show a similar pattern, but with reduced amplitude of deflection. At T_e = 40 km the deflection becomes negligible.

7.2. Breaking of a Continuous Plate as a Possible Uplift Mechanism

The evidence above suggests that the main uplift phase of the TAM was not related to the main extension phase of the Ross Embayment but rather to a minor transtensional movement between East and West Antarctica during early Tertiary plate reorganizations. A transtensional boundary does not require the existence of rift basins along the entire mountain front and is in agreement with steep lateral variations in crustal thickness. In addition, a model in which East Antarctica flexes independently of West Antarctica fits well both the gravity and the topography (Figure 10). We therefore argue that mechanisms involving isostatic rebound due to stretching of the lithosphere [*Bott and Stern*, 1992; *Chéry et al.*, 1992; *van der Beek et al.*, 1994] cannot explain the uplift of the TAM. On the other hand, heat conduction or advection from the extended upper mantle of the Ross Embayment into the edge of a cratonic upper mantle of East Antarctica following the rifting in the Ross Embayment would not explain uplift that began 30 Myr after the cessation of rifting. Also there is no reported volcanic activity during the early Tertiary which could be coeval with the initiation of uplift.

The only tectonic or magmatic event coeval with the initiation of uplift is the plate reorganization in the Southern Ocean which may have temporarily induced a transtensional motion between East and West Antarctica. The kinematic shearing involved in this motion could have facilitated fault zone weakening and high pore pressure development, thus allowing frictionless slip to occur within a steep fault zone. Additional weakening of the boundary could have been caused by increased heat input from small-scale convection established a few million years after a steep lateral thermal gradient would have been created [e.g., *Buck*, 1986] as a result of the rifting and thinning of the Ross Embayment lithosphere. The fault zone could have then acted to decouple the lithospheres of West and East Antarctica, allowing the release of stresses and

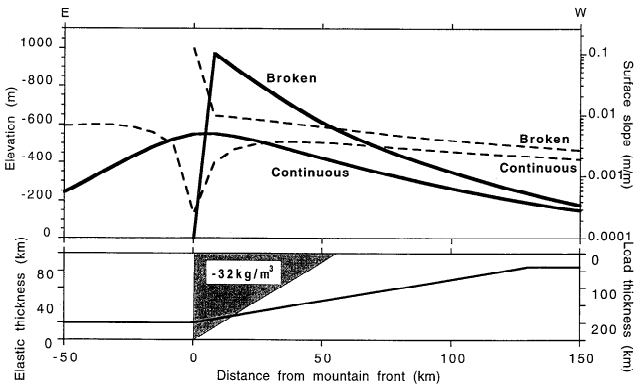

Figure 13. (top) Comparison of elevation (solid lines) and surface slope (dashed lines) generated by 2-D finite difference thin elastic plate models with two different boundary condition, a continuous plate, and a broken plate at $x = 0$. (bottom) Lateral distribution of the load and elastic thickness used to generate these models. The load used for this model is smaller than the "thermal buoyancy" load used in Figure 7 to represent a shorter time between the end of Ross Embayment extension and 55 Ma, and erosional rebound was assumed to be negligible. The model illustrates that breaking of a loaded elastic plate leads to an abrupt increase in elevation and surface slope, which are expected to increase significantly the rates of erosion, rock uplift, and exhumation.

thermal bending moments within the East Antarctic lithosphere and allowing a rebound of the free edge. Stresses could have accumulated during the rifting episode [e.g., *van der Beek et al.*, 1994] or subsequently as the edge of the East Antarctic lithosphere was being heated.

A breaking of the plate by the transtensional motion would have created two immediate changes: First, the amount of surface uplift would have almost doubled (Figure 13), and second, the slope of the escarpment which bounds the uplift would have become steeper by an order of magnitude or more. Because erosion is a function of elevation and particularly of the topographic slope [e.g., *Tucker and Slingerland*, 1994], the rate of erosion at the mountain front is expected to have accelerated considerably due to this change. The erosion would have caused rapid exhumation of buried rocks and at the same time would have enforced additional rock uplift by isostatic rebound. The initiation of uplift of the TAM at 55 Ma was determined by identifying a break in the slope of the apparent age profile of apatite fission tracks [*Fitzgerald*, 1994]. This break in slope signals the onset of rapid cooling due to denudation [*Fitzgerald*, 1994]. Therefore the initiation of the TAM uplift was in fact the beginning of rapid exhumation. We hypothesize that the change from an unbroken to a broken plate in the early Tertiary, caused by a minor transtensional event, created rapid surface and rock uplift and rapid exhumation, and the rapid exhumation was detected by the fission track method as the initiation of uplift.

8. Other Aspects of the Geology and Glacial History of East Antarctica

8.1. Extent of Beacon Sediments Under the Ice Cap

Having estimated a value for T_e and for the preflexural elevation by considering free air gravity, the structure of the region covered by EAST93 can now be examined in more detail. A model including structure below the ice-rock interface is shown in Figure 14, together with observed and calculated free air gravity anomalies. The model shown in Figure 14 incorporates all of the features shown in Figure 9 (though for clarity only the upper part of the model is shown) and has an elastic thickness $T_e = 85$ km, a preflexural elevation of 700 m, and a crustal thickness of 45 km in East Antarctica. The upper surface of the crust is a combination of the subglacial topography determined from EAST93 data, an approximation to topography within the TAM, and the flexure profile elsewhere. The shape of the base of the crust (Moho) is exactly that of the flexure profile with $T_e = 85$ km.

The calculated gravity represented by the dashed profile in Figure 14a is for a model in which the East Antarctic crust is uniform throughout its entire depth with an average continental crustal density of 2830 kg/m^3 [*Christensen and Mooney*, 1995]. The fit to the residual free air anomalies from EAST93 is good, but where subglacial peaks occur, the calculated anomalies are consistently higher than those observed. To reduce these peaks (solid profile, Figure 14a), a layer of lower density rock representing Beacon Supergroup sediments is included in the crust (Figure 14b). The density of that layer is 2400 kg/m^3, consistent with laboratory density measurements of Beacon Supergroup rocks [*Barrett and Froggatt*, 1978]. Owing to the limited lateral extent of these peaks, the reduced density was included in the model as an uncompensated body.

By subtracting the elevation of the base of the Beacon sediments in Figure 14b from the flexural curve in Figure 9b we can derive a minimum thickness of the Beacon Supergroup sediments. It is significant that the body representing the Beacon sediments thins away from the TAM (Figure 15), as this gives some indication of the likely geology that would be encountered toward the Wilkes Basin. Reconstruction of a composite sedimentary facies of the Beacon Supergroup from different outcrops throughout the TAM indicates that the sedimentary section indeed thins away from West Antarctica [*Collinson*, 1991]. *Collinson* [1991] suggested that the upper part of the Beacon Supergroup rocks was deposited in a foreland basin. The large width (270 km) of the inferred sediment section and its shape are in agreement with the shape and dimensions of foreland basins deposited over a rigid lithosphere such as the Appalachian and the Alberta Basins [*Tankard*, 1986] and the Taranaki Foreland Basin [*Holt and Stern*, 1994]. Another conclusion from Figure 15 is that on a regional basis the Kukri peneplain, which comprises the base of the Beacon Supergroup, was not horizontal prior to the TAM uplift but was dipping eastward about 0.5°. One should therefore apply a correction of about 0.5° to the Kukri peneplain when calculating post-Paleozoic tilting.

The above interpretation is only valid if the long-wavelength bedrock topography is due to flexure and not due to a long-wavelength erosional component. Seismic stratigraphic mapping under the traverse will be needed to evaluate the erosional component. We should also qualify our interpretation by pointing out that our model is 2-D. It is possible to produce an apparent density reduction of the peaks if the width of the features (perpendicular to the profiles) are less than about three ice thicknesses. The regional subsurface topography [*Drewry*, 1983] does not show elongate features parallel to the traverse, but final verification should await detailed mapping.

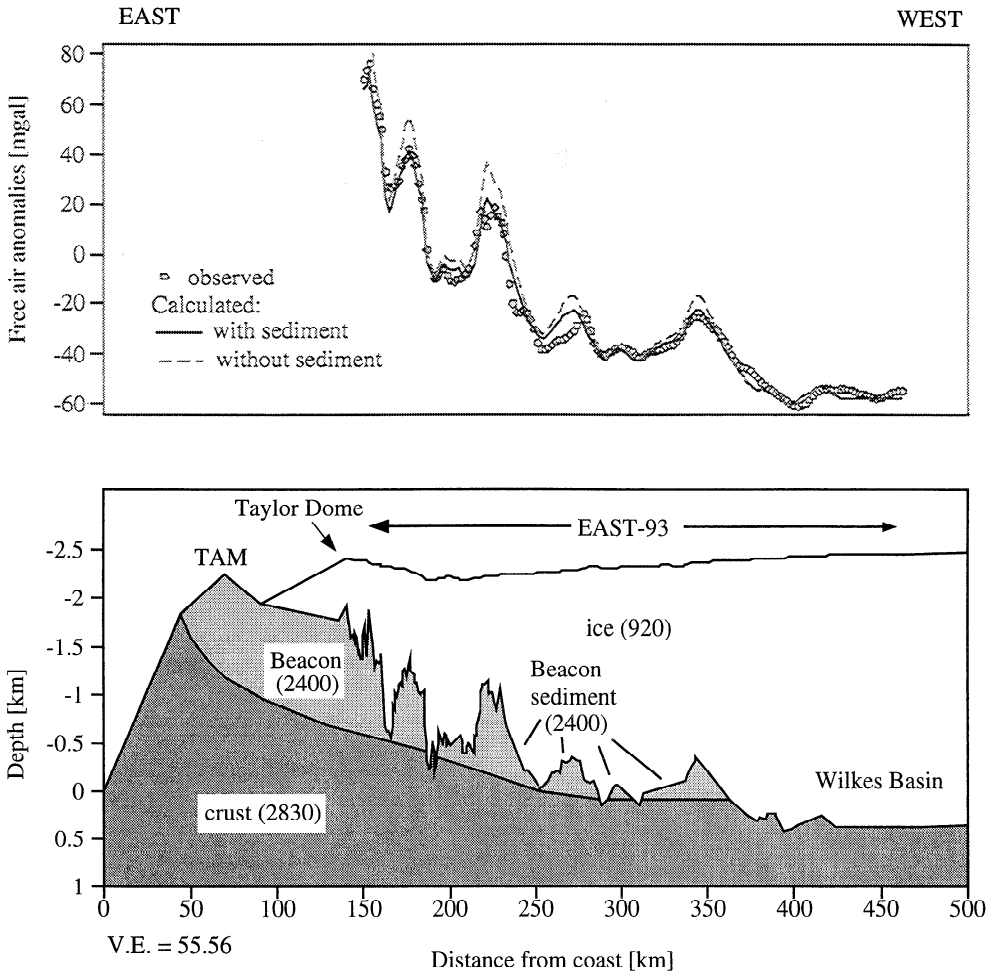

Figure 14. Gravity model with and without a near-surface low-density layer representing the Beacon Supergroup sediments. (a) Comparison between observed gravity anomaly from Figure 5b and calculated gravity anomaly with and without the low-density layer. (b) A model of the shallow subice structure under the TAM and the Wilkes Basin with densities in kg/m^3. Ice surface and bedrock elevations along the EAST93 traverse are from Figure 5. The topography of the TAM and the base of the Beacon (Kukri peneplain) from the coast inland to a distance of 70 km is simplified after maps of *Warren* [1969], *McElroy and Rose* [1987], and *Woolfe et al.* [1989] and other maps and has little effect on the modeled gravity. The base of the Beacon under the ice sheet is adjusted to minimize the magnitude of the peaks in the dashed gravity profile. The Moho follows a flexural surface with T_e = 85 km, and the preuplift elevation of East Antarctica is 700 m.

8.2. Gravity and the Glacial History of East Antarctica

8.2.1. Cenozoic sediments in Wilkes Basin. The presence or absence of Cenozoic marine sediments in the Wilkes Basin is the centerpiece of the current debate about the history of the East Antarctic ice sheet and the recent uplift of the TAM [*Webb*, 1990; *Clapperton and Sugden*, 1990]. One school of thought ascribes to the view that the East Antarctic ice sheet collapsed in the late Miocene and early Pliocene to allow a marine incursion into Wilkes Basin [*Webb*, 1990]. During the subsequent glaciation, marine diatoms (youngest of Pliocene age) were glacially transported uphill and deposited at an elevation of 1.5–4.5 km in the TAM to form the Sirius Formation [*Webb*, 1990]. The alternative and more traditional view is that a large ice sheet existed over Antarctica during the Miocene and Pliocene and the diatoms reached high elevations by being wind-blown onto the ice sheet and incorporated locally in tills.

Drewry [1976] and *Steed* [1983] interpreted the negative free air gravity anomaly (collected during the International Geophysical Year (IGY)) in conjunction with magnetic anomaly data over the basin, to indicate a 2- to 3-km-thick sedimentary layer of relatively low-density within the basin. Our gravity and magnetic data are far more detailed and accurate than previously available data and do not require the existence of additional low-density and low-susceptibility material (see below) representing Cenozoic sediments along any part of the profile, including the Wilkes Basin. The gravity anomaly can be completely accounted for by flexure of the East Antarctic plate and the existence of Beacon-type sediments which thin toward the Wilkes Basin (Figure 13a). *ten Brink and Stern* [1992] have also argued that the negative gravity anomaly could not be produced solely by low-density sediments filling a "rifted" Wilkes basin, because sediments filling a several hundred kilometer-

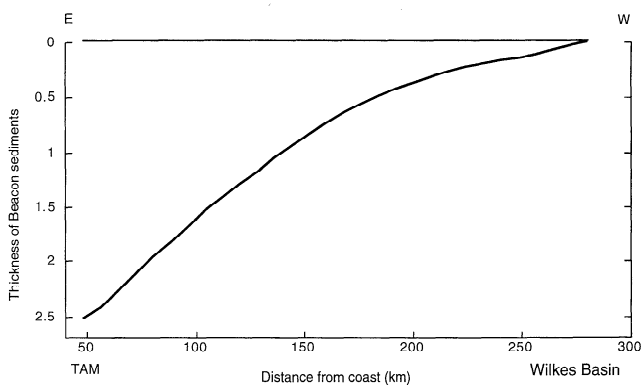

Figure 15. Minimum thickness of Beacon sediments derived by subtracting the elevation of the base of the Beacon sediments in Figure 14b from the flexural curve in Figure 9b. If the reference elevation prior to the flexural uplift of the TAM was flat, then the base of the Beacon sediments (the Kukri peneplain) at that time deepened at 0.5° toward the coast.

wide basin must be locally compensated and will therefore have a zero gravity anomaly at the basin's center.

8.2.2. Glacial rebound. *Bentley* [1983] and *Steed* [1983] discussed the origin of the negative gravity anomaly over the Wilkes Basin and as one of their hypotheses suggested an incomplete glacial rebound due to melting. *Greischar et al.* [1992] identified a long-wavelength negative free air anomaly of ~17 mGal in the Ross Embayment, which they attributed to the removal of a thick ice sheet over that area during the last glacial period. Sea level measurements along the East Antarctic coast have led *Zwartz et al.* [1996] to suggest that melting and ice sheet retreat occurred in the East Antarctic ice sheet since the last glacial period. On the other hand, drill core data in the interior of East Antarctica indicate little change in the interior elevation of the ice sheet [*Jouzel et al.*, 1989], and studies of glacial drift in the higher reaches of several of the larger outlet glaciers of the TAM suggest that the plateau elevation in the interior was no greater than 100 m higher than today [e.g., *Denton et al.*, 1989].

In our gravity modeling, we assigned a zero gravity anomaly to the reference crustal structure of East Antarctica (Figure 6). The calculated gravity did not require a subsequent constant shift or the removal of a gradient to fit the data. In other words, we did not find any residual long-wavelength anomalies in the data that could be interpreted as incomplete glacial rebound. This statement is provisional upon the interpretation of long-wavelength contributions in our model as being due to sources other than glacial rebound: We subtracted the degree 2–10 gravity field from the data because it is believed to arise from deep mantle heterogeneities [*Bowin*, 1991]. The contrast of upper mantle density between East and West Antarctica in our model produced a long-wavelength negative anomaly (Figure 6), but this contrast fits well with other elements of the model.

8.3. Extent of the Ferrar Magmatic Province: A Magnetic Model

A magnetic model was constructed in an attempt to give some indication of the magnetic structure inland of the TAM. No attempt was made to fully model the magnetic profile because the number of unknown variables (polarity, declination, induced magnetization, etc.) involved with modeling a single 2-D profile is large. Nevertheless, we can test a few simple models to learn about the depth of the magnetic source (Figure 16).

We start by assigning a uniform low magnetization (susceptibility $k' = 0.005$ cgs units) to the crust and the sediments down to 10 km. The calculated magnetic field ("uniform" curve in Figure 16a) is affected by the topography. The fit is good at the eastern end of the line (km 150–190) because of the high-amplitude topography and its proximity to the surface, but it is poor elsewhere. In particular, the observed anomaly around km 220 from the coast is negative, whereas the calculated anomaly is positive. This misfit indicates the existence of reversely magnetized rocks under the profile.

Next we vary the susceptibility laterally while maintaining magnetization to a depth of 10 km. In particular, the area around km 220 is assigned negative susceptibility reflecting remnant magnetization there. The calculated anomaly ("variable deep" in Figure 16a) is now negative, but its wavelength is much larger than observed. This misfit suggests that the negative anomaly is concentrated near the ice-bedrock interface. A 200-nT step observed in the data around km 360 can, however, be modeled as a small contrast (0.001) in crustal susceptibility k' down to 10 km.

Our final and preferred model is one in which the suscepti-

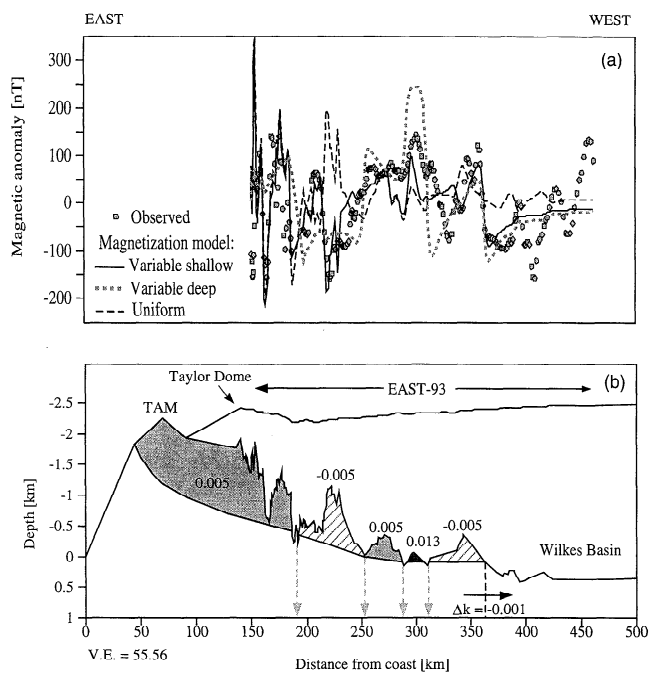

Figure 16. Magnetic model along the EAST93 traverse. (a) Comparison between observed magnetic anomaly from Figure 5c and calculated magnetic anomaly from various models discussed in text. Gray line, "uniform," model with a constant susceptibility in the upper 10 km of rock column. Gray squares, "variable deep," model with variable susceptibilities down to 10 km deep. The lateral distribution of susceptibility (in cgs units) is shown in Figure 16b but is extended down along vertical boundaries to 10 km deep (gray dashed arrows in Figure 16b). Solid line, "variable shallow," model with shallow variable susceptibility (shaded areas in Figure 16b) and a susceptibility contrast to 10 km depth at km 360. (b) Geometry of magnetic model. The magnetized region overlaps the distribution of the Beacon sediments (in Figure 13b) because dolerite sills and dikes are mainly emplaced in the sedimentary section and only locally in pre-Devonian basement.

bility is concentrated near the bedrock surface and is laterally variable. For modeling convenience and for lack of better constraints, the near-surface susceptibility overlaps the distribution of the Beacon sedimentary section from the gravity model. Although they are nonmagnetic, the Beacon sediments are pervasively and massively intruded in the TAM by Ferrar dolerite sills and Kirkpatrick basalt flows, whereas the underlying basement is much less intruded (Figure 2). The underlying crust is assigned zero susceptibility and a crustal susceptibility contrast of -0.001 exists at km 360. A susceptibility value of $k' = 0.005$ (cgs units) was chosen to reflect an average susceptibility for the rocks of the Beacon Supergroup which are made up of weakly magnetized sediments ($k' \approx 0$) and the more magnetized dolerite ($k' \approx 0.013$ [*Dobrin and Savit*, 1988]) of the Ferrar Supergroup. The calculated model ("variable shallow" in Figure 16a) fits the observed data better than the other models; in particular, the wavelength of the positive and negative anomalies between km 180 and 250 is similar to the observed data. Further improvements to the model are not warranted because of the lack of constraints.

The Ferrar dolerites appear to be confined to a linear belt parallel to the Ross Embayment and inboard of the paleo-Pacific convergent plate margin, but the linear exposure may be an artifact of the distribution of rock outcrops along the TAM, which uplifted much later. The final magnetic model of Figure 16b indicates that the observed magnetic anomalies are best explained by magnetization of near-surface rocks to a distance of at least 250 km from the East–West Antarctic boundary, where the negative anomaly ends, and probably to a distance of 350 km. Because the only near-surface known magnetized sources in the area are the Ferrar Dolerites and the Kirkpatrick basalts, we conclude that the Ferrar volcanic province in southern Victoria Land is at least 250 km and possibly 350 km wide. This estimate is at least double the width previously assumed [*Elliot*, 1992]. An extensive subglacial mesa topography in the south pole sector has been interpreted as Beacon Supergroup with intruded Ferrar sills [*Drewry*, 1976], also suggesting a wider distribution for the province. The width of this province is similar to other voluminous linear volcanic provinces which erupted over a short period of time along the east coast of the United States [*Holbrook and Kelemen*, 1993] and along the North Atlantic margins [*White*, 1992].

Between km 370 and 400 from the coast, a region of flat negative anomalies gives way to anomalies that become positive toward the end of the traverse. Although we did not model this increased anomaly, we hypothesize that it too reflected crustal susceptibility changes. A transition toward a positive magnetic anomaly in the interior of East Antarctica, located parallel to the TAM along the western side of the Wilkes Basin, was observed in the POGO [*Steed*, 1983] and Magsat [*von Frese et al.*, 1994] satellite data and by aeromagnetic measurements in northern Victoria Land [*Bosum et al.*, 1989]. This transition was interpreted to mark the boundary between orogenic belts developed on the margin of the East Antarctic shield and the positive anomaly associated with the shield itself [*Steed*, 1983; *Bosum et al.*, 1989].

9. Summary

1. Detailed subglacial topography and gravity measurements from a geophysical traverse conducted in 1993/1994 from the Transantarctic Mountains (TAM) to the hinterland Wilkes Basin confirm the origin of the TAM as a flexural uplift of the edge of East Antarctica.

2. The topography and the gravity data can be jointly fit by a broken elastic plate model having an elastic thickness of 85 ± 15 km and a preuplift elevation of 700 ± 50 m for East Antarctica.

3. Analysis of isostatic support of loads close to the TAM-Ross Embayment boundary indicates very low lithospheric strength at that boundary, in support of a free edge model.

4. We argue that rapid uplift of the TAM occurred 30 Myr after the extension of the adjacent Ross Embayment and that rift basins adjacent to the TAM are rare. We suggest that transtensional motion between East and West Antarctica due to Southern Ocean plate reorganization triggered the uplift by breaking the elastic plate at the mountain front. The increased elevation and surface slope resulting from this change accelerated the rates of erosion and exhumation, which were documented by apatite fission track analysis as the initiation of uplift.

Other results pertaining to the geology and glacial history of East Antarctica are as follows:

1. Magnetic data indicate that the Ferrar flood basalts extend at least 250–350 westward from the TAM–Ross Embayment boundary.

2. Gravity data indicate that the Beacon Supergroup of Paleozoic and Mesozoic sediments thin gradually under the ice to a distance of 300 km from that boundary.

3. The gravity data do not require the presence of sediments in the Wilkes Basin, in contrast to suggestions made in support of Pliocene melting of the ice sheet.

4. The gravity data show isostatic support for the present-day ice sheet load and do not require significant melting since the last glacial period.

Acknowledgments. We thank the following people for their contributions to the success of the experiment: Dale Benson and Larry Hotham, USGS-NMD, for accurately locating reference points; John West, New Zealand Department of Survey and Land Information, for an outstanding survey of the traverse; Ed Waddington and Dave Morse, University of Washington, and Steve Hodge, USGS-WRD, for sharing their hardware, software, and design of their radar system; Eivind Rygg and Norsk-Hydro Co., Norway, for lending the snow streamer; Rob Huggins and Geometrics for supplying the R60 Strataview seismic recording system; and Bill Robinson and John Behrendt, USGS, for helping with equipment. We thank the personnel at McMurdo Station and at the Taylor Dome drill site for their excellent support during the experiment and the Scott Base personnel for their hospitality and help in mobilizing and demobilizing the experiment. We also thank the New Zealand Air Force for carrying out precision airdrops of explosives at the caches and the U.S. Navy VXE-6 squadron and Ken Borek Air for their logistical support. The experiment would not have succeeded without the efforts of our field team Mike Collins, Jon de Vries, Raffi Katzman, Bill King, David King, and John West. Raffi Katzman, John Harris, and Myung Lee helped with initial data processing and Jeremy Loss helped with drafting. Carl Bowin supplied the gravity field for degree 2–10 along the traverse, Don McKnight made the Scott Base and IGRF-1990 magnetic data available, and Hans Schouten guided us in the magnetic modeling. Bill Dillon and Bob Oldale reviewed the manuscript. We thank Larry Lawver, Charles Bentley, and an anonymous Associate Editor for their thorough reviews. Funding was obtained from the Foundation of Research Science and Technology (NZ), the National Science Foundation grant OPP92-20462, and the U.S. Geological Survey. R. I. H. was also supported by the New Zealand Commonwealth Scholarship and Fellowship plan.

References

Anderton, P. W., Great South and Campbell basins, New Zealand: Evaluation of geology and hydrocarbon potential, *Far East Rep. 828*, Phillips Pet. Co., Singapore, 1982.

ANTOSTRAT Project, Seismic stratigraphic atlas of the Ross Sea, Antarctica, in *Geology and Seismic Stratigraphy of the Antarctic Margin, Antarct. Res. Ser.*, vol. 68, edited by A. K. Cooper et al., 22 plates, AGU, Washington, D. C., 1995.

Barrett, P. J., and P. C. Froggatt, Densities, porosities and seismic velocities of some rocks from Victoria Land, Antarctica, *N. Z. J. Geol. Geophys.*, *21*(2), 175–187, 1978.

Barrett, P. J., D. H. Elliot, and J. F. Lindsey, The Beacon Supergroup (Devonian-Triassic) and Ferrar Group (Jurassic) in the Beardmore Glacier area, Antarctica, in *Geology of the Central Transantarctic Mountains, Antarct. Res. Ser.*, vol. 36, edited by M. D. Turner and J. F. Splettstoesser, pp. 339–428, AGU, Washington, D. C., 1986.

Barrett, P. J., M. J. Hambrey, D. M. Harwood, A. R. Pyne, and P.-N. Webb, Synthesis—Antarctic Cenozoic history from the CIROS-1 drill hole, McMurdo Sound, *DSIR Bull.*, *245*, 241–251, 1989.

Behrendt, J. C., and A. K. Cooper, Evidence of rapid Cenozoic uplift of the shoulder escarpment of the Cenozoic West Antarctic rift system and a speculation on possible climate forcing, *Geology*, *19*, 315–319, 1991.

Bentley, C. R., The structure of Antarctica and its cover, in *Solid Earth and Interface Phenomena, Res. Geophys.*, vol. 2, edited by H. Odishaw, pp. 335–389, Mass. Inst. of Technol., Cambridge, 1964.

Bentley, C. R., Crustal structure of Antarctica from geophysical evidence—A review, in *Antarctic Earth Science—Proceedings of the Fourth International Symposium on Antarctic Earth Sciences*, edited by R. L. Oliver, P. R. James, and J. B. Jago, pp. 491–497, Cambridge Univ. Press, New York, 1983.

Bentley, C. R., Configuration and structure of the subglacial crust, in *The Geology of Antarctica*, edited by R. J. Tingey, pp. 335–364, Oxford Univ. Press, New York, 1991.

Berg, J., R. J. Moscati, and D. L. Herz, A petrologic geotherm from a continental rift in Antarctica, *Earth Planet. Sci. Lett.*, *93*, 98–108, 1989.

Blackman, D. K., R. P. Von Herzen, and L. A. Lawver, Heat flow and tectonics in the western Ross Sea, in *The Antarctic Continental Margin, Geology and Geophysics of the Western Ross Sea, Earth Sci. Ser.*, vol. 5B, edited by A. K. Cooper and F. J. Davey, pp. 179–190, Circum-Pac. Counc. for Energy and Miner. Resour., Houston, Tex., 1987.

Bodine, J. H., M. S. Steckler, and A. B. Watts, Observations of flexure and the rheology of the oceanic lithosphere, *J. Geophys. Res.*, *86*, 3695–3707, 1981.

Borg, S. C., D. J. DePaolo, and B. M. Smith, Isotopic structure and tectonics of the central Transantarctic Mountains, *J. Geophys. Res.*, *95*, 6647–6667, 1990.

Bosum, W., D. Damaske, N. W. Roland, J. Behrendt, and R. Saltus, The GANOVEX IV Victoria Land/Ross Sea aeromagnetic survey: Interpretation of anomalies, *Geol. Jahrb. Reihe E*, *38*, 153–230, 1989.

Bott, M. H. P., and T. A. Stern, Finite element analysis of Transantarctic Mountain uplift and coeval subsidence in the Ross Embayment, *Tectonophysics*, *201*, 341–356, 1992.

Bowin, C., Earth's gravity field and plate tectonics, *Tectonophysics*, *187*, 69–81, 1991.

Buck, W. R., Small-scale convection induced by passive rifting, the cause for uplift of rift shoulders, *Earth Planet. Sci. Lett.*, *77*, 362–372, 1986.

Cande, S. C., C. A. Raymond, J. Stock, and W. F. Haxby, Geophysics of the Pitman Fracture Zone and Pacific-Antarctic plate motion during the Cenozoic, *Science*, *270*, 947–953, 1995.

Carslaw, H. S., and J. G. Jaeger, *Conduction of Heat in Solids*, 2nd ed., 510 pp., Oxford Univ. Press, Oxford, 1959.

Chéry, J., F. Lucazeau, M. Daignières, and J. P. Vilotte, Large uplift of rift flanks: A genetic link with lithospheric rigidity?, *Earth Planet. Sci. Lett.*, *112*, 195–211, 1992.

Christensen, N. I., and W. D. Mooney, Seismic velocity structure and composition of the continental crust: A global review, *J. Geophys. Res.*, *100*, 9761–9788, 1995.

Clapperton, C. M., and D. E. Sugden, Late Cenozoic glacial history of the Ross Embayment, Antarctica, *Quat. Sci. Rev.*, *9*, 253–272, 1990.

Collinson, J. W., The paleo-Pacific margin as seen from East Antarctica, in *Geological Evolution of Antarctica*, edited by M. R. A. Thomson, et al., pp. 199–204, Cambridge Univ. Press, New York, 1991.

Cooper, A. K., F. J. Davey, and K. Hinz, Crustal extension and origin of sedimentary basins beneath the Ross Sea and the Ross Ice Shelf, Antarctica, in *Geological Evolution of Antarctica*, edited by M. R. A. Thompson et al., pp. 285–291, Cambridge Univ. Press, New York, 1991.

Crary, A. P., Results of United States traverses in East Antarctica, 1958–61, *IGY Int. Geophys. Year Glaciol. Rep. 7*, Am. Geogr. Soc., New York, 1963.

Denton, G. H., J. G. Bockheim, S. C. Wilson, J. E. Leide, and B. G. Andersen, Late Quaternary fluctuations of the Beardmore Glacier, Transantarctic Mountains, *Quat. Res.*, *31*, 183–209, 1989.

Dobrin, M. B., and C. Savit, *Introduction to Geophysical Prospecting*, McGraw-Hill, New York, 1988.

Drewry, D. J., Sedimentary basins of the East Antarctic craton from geophysical evidence, *Tectonophysics*, *36*, 301–314, 1976.

Drewry, D. J., Ice flow, bedrock, and geothermal studies from radio-echo sounding inland of McMurdo Sound, Antarctica, in *Antarctic Geoscience*, edited by C. Craddock, pp. 977–983, Univ. of Wis. Press, Madison, 1982.

Drewry, D. J., *Antarctica: Glaciological and Geophysical Folio*, Scott Polar Res. Inst., Cambridge, England, U. K., 1983.

Elliot, D. H., Jurassic magmatism and tectonism associated with Gondwanaland break-up: an Antarctic perspective, in *Magmatism and the Causes of Gondwana Break-up*, edited by B. Storey, T. Alabaster, and P. J. Pankhurst, *Geol. Soc. Spec. Publ. London*, *68*, 165–184, 1992.

Fitzgerald, P. G., The Transantarctic Mountains of southern Victoria Land: The application of apatite fission track analysis to a rift shoulder uplift, *Tectonics*, *11*, 634–662, 1992.

Fitzgerald, P. G., Thermochronologic constraints on post-Paleozoic tectonic evolution of the central Transantarctic Mountains, Antarctica, *Tectonics*, *13*, 818–836, 1994.

Fitzgerald, P. G., M. Sandiford, P. J. Barrett, and A. J. W. Gleadow, Asymmetric extension associated with uplift and subsidence in the Transantarctic Mountains and Ross Embayment, *Earth Planet. Sci. Lett.*, *81*, 67–78, 1986.

Fitzpatrick, J. J., Preliminary report on the physical and stratigraphic properties of the Taylor Dome ice core, *Antarct. J. U.S.*, *29*(5), 84–86, 1994.

Greischar, L. L., C. R. Bentley, and L. R. Whiting, An analysis of gravity measurements on the Ross Ice Shelf, Antarctica, in *Contributions to Antarctic Research III, Antarct. Res. Ser.*, vol. 57, edited by D. H. Elliot, pp. 105–155, AGU, Washington, D. C., 1992.

Hackney, R. I., Geophysical investigation of the Wilkes subglacial basin, East Antarctica, M.Sc. thesis, Victoria Univ. of Wellington, New Zealand, 1996.

Heimann, A., T. H. Fleming, D. H. Elliot, and K. A. Foland, A short interval of Jurassic continental flood basalt volcanism in Antarctica as demonstrated by $^{40}Ar/^{39}Ar$ geochronology, *Earth Planet. Sci. Lett.*, *121*, 19–41, 1995.

Holbrook, W. S., and P. B. Kelemen, Large igneous province on the U.S. Atlantic margin and implications for magmatism during continental breakup, *Nature*, *364*, 433–436, 1993.

Holt, W. E., and T. A. Stern, Subduction, platform subsidence, and foreland thrust loading: The Late Tertiary development of Taranaki Basin, New Zealand, *Tectonics*, *13*, 1068–1092, 1994.

Jouzel, J., G. Raisbeck, J. P. Benoist, F. Yiou, C. Lorius, D. Raynaud, J. R. Petit, N. J. Barkov, Y. S. Korotkevitch, and V. M. Kotlyakov, A comparison of deep Antarctic ice cores and their implications for climate between 65,000 and 15,000 years ago, *Quat. Res.*, *31*, 135–160, 1989.

Langel, R., International Geomagnetic Reference Field, 1991 revision: International Association of Geomagnetism and Aeronomy (IAGA) Division V, Working Group 8: Analysis of the main field and secular variation, *Phys. Earth Planet. Inter.*, *70*, 1–6, 1992.

Lawver, L. A., L. M. Gahagan, and M. F. Coffin, The development of paleoseaways around Antarctica, in *The Antarctic Paleoenvironment: A Perspective on Global Change, Antarct. Res. Ser.*, vol. 56, edited by J. P. Kennett and D. A. Warnke, pp. 7–30, AGU, Washington, D. C., 1992.

Lyon-Caen, H., and P. Molnar, Constraints on the deep structure and dynamic processes beneath the Alps and adjacent regions from an analysis of gravity anomalies, *Geophys. J. Int.*, *99*, 19–32, 1989.

McElroy, C. T., and G. Rose, Geology of the Beacon Heights area, southern Victora Land, Antarctica, scale 1:50,000, *Misc. Ser. Map 15*, N. Z. Geol. Surv., Wellington, 1987.

Molnar, P., T. Atwater, J. Mammerickx, and S. M. Smith, Magnetic anomalies, bathymetry, and the tectonic evolution of the South Pacific since Late Cretaceous, *Geophys. J. R. Astron. Soc.*, *40*, 383–420, 1975.

O'Connell, D. R. H., and T. M. Stepp, Structure and evolution of the crust at the Transantarctic Mountains–Ross Sea crustal transition: Results from the Tourmaline Plateau seismic array of the GANOVEX V ship-to-shore seismic refraction experiment, *Geol. Jahrb.*, *47*, 229–276, 1993.

Robinson, E. S., and J. F. Splettstoesser, Structure of the Transantarctic Mountains determined from geophysical surveys, in *Geology of the Central Transantarctic Mountains*, *Antarct. Res. Ser.*, vol. 36, edited by M. D. Turner and J. F. Splettstoesser, pp. 119–162, AGU, Washington, D. C., 1984.

Roult, G., D. Rouland, and J. P. Montagner, Antarctica, 2, Uppermantle structure from velocities and anisotropy, *Phys. Earth Planet. Inter.*, *84*, 33–57, 1994.

Royer, J. Y., and D. T. Sandwell, Evolution of the Indian Ocean since the Late Cretaceous: Constraints from Geosat altimetry, *J. Geophys. Res.*, *94*, 13,755–13,782, 1989.

Smith, A. G., and D. J. Drewry, Delayed phase change due to hot asthenosphere causes Transantarctic uplift?, *Nature*, *309*, 536–538, 1984.

Spence, G. D., and I. Asudeh, Seismic velocity structure of the Queen Charlotte Basin beneath Hecate Strait, *Can. J. Earth Sci.*, *30*, 787–805, 1993.

Steed, R. H. N., Structural interpretation of Wilkes Land, Antarctica, in *Antarctic Earth Science—Proceedings of the Fourth International Symposium on Antarctic Earth Sciences*, edited by R. L. Oliver, P. R. James, and J. B. Jago, pp. 567–572, Cambridge Univ. Press, New York, 1983.

Stern, T. A., and U. S. ten Brink, Flexural uplift of the Transantarctic Mountains, *J. Geophys. Res.*, *94*, 10,315–10,330, 1989.

Sugden, D. E., G. H. Denton, and D. R. Marchant, Landscape evolution of the Dry Valleys, Transantarctic Mountains: Tectonic implications, *J. Geophys. Res.*, *100*, 9949–9967, 1995.

Sutherland, R., The Australia-Pacific boundary and Cenozoic plate motion in the SW Pacific: Some constraints from Geosat data, *Tectonics*, *14*, 819–831, 1995.

Tankard, A. J., On the depositional response to thrusting and lithospheric flexure: Examples from the Appalachian and Rocky Mountain basins, in *Foreland Basins*, edited by P. A. Allen and P. Homewood, *Spec. Publ. Int. Assoc. Sedimentol.*, *8*, 364–394, 1986.

ten Brink, U. S., and S. Bannister, EAST93—Geophysical traverse from the Transantarctic Mountains to the Wilkes Basin, East Antarctica, *U.S. Geol. Surv. Open File Rep.*, *95-225*, 1995.

ten Brink, U. S., and T. A. Stern, Rift flank uplifts and hinterland basins: comparison of the Transantarctic Mountains with the Great Escarpment of southern Africa, *J. Geophys. Res.*, *97*, 569–585, 1992.

ten Brink, U. S., S. Bannister, B. C. Beaudoin, and T. A. Stern, Geophysical investigations of the tectonic boundary between East and West Antarctica, *Science*, *261*, 45–50, 1993.

Tessenshon, F., The Ross Sea region, Antarctica: Structural interpretation in relation to the evolution of the Southern Ocean, *Terra Antarct.*, *1*, 553–558, 1994.

Todd, B. J., I. Reid, and C. E. Keen, Crustal structure across the southwest Newfoundland transform margin, *Can. J. Earth Sci.*, *25*, 744–759, 1988.

Tucker, G. E., and R. L. Slingerland, Erosional dynamics, flexural isostasy, and long-lived escarpments: A numerical modeling study, *J. Geophys. Res.*, *99*, 12,229–12,243, 1994.

van der Beek, P., S. Cloetingh, and P. Andriessen, Mechanisms of extensional basin formation and vertical motion at rift flanks: Constraints from tectonic modelling and fission track thermochronology, *Earth Planet. Sci. Lett.*, *121*, 417–433, 1994.

von Frese, R. R. B., D. E. Alsdorf, J.-H. Kim, T. M. Stepp, D. R. H. O'Connell, K. J. Hayden, and W.-S. Li, Regional geophysical imaging of the Antarctic lithosphere, in *Recent Progress in Antarctic Earth Sciences*, edited by Y. Yoshida, K. Kaminuma, and K. Shiraishi, pp. 465–474, TERRAPUB, Tokyo, 1994.

Waddington, E. D., D. L. Morse, and G. D. Clow, Glacier geophysics at Taylor Dome: Year 4, *Antarct. J. U.S.*, *29*(5), 82–84, 1994.

Walcott, R. I., Flexural rigidity, thickness and viscosity of the lithosphere, *J. Geophys. Res.*, *75*, 3941–3954, 1970.

Warren, G., Terra Nova Bay McMurdo Sound area, in *Antarctic Map Folio Series*, edited by V. C. Bushnell and C. Craddock, scale 1: 1,000,000, Folio 12, Plate 13, sheet 14, Am. Geogr. Soc., New York, 1969.

Webb, P. N., The Cenozoic history of Antarctica and its global impact, *Antarct. Sci.*, *2*, 3–21, 1990.

Weissel, J. K., and G. D. Karner, Flexural uplift of rift flanks due to mechanical unloading of the lithosphere during extension, *J. Geophys. Res.*, *94*, 13,919–13,950, 1989.

White, R. S., Crustal structure and magmatism of North Atlantic continental margins, *J. Geol. Soc. London*, *149*, 841–853, 1992.

Wilson, T. J., Cenozoic transtension along the Transantarctic Mountains–West Antarctic rift boundary, southern Victoria Land, Antarctica, *Tectonics*, *14*, 531–545, 1995.

Woolfe, K. J., P. A. Kirk, and A. M. Sherwood, Geology of the Knobhead area, southern Victora Land, Antarctica, *Misc. Ser. Map 15*, scale 1:50,000, N. Z. Geol. Surv., Wellington, 1989.

Zuber, M. T., T. D. Bechtel, and D. W. Forsyth, Effective elastic thicknesses of the lithosphere and mechanisms of isostatic compensation in Australia, *J. Geophys. Res.*, *94*, 9353–9367, 1989.

Zwartz, D. P., K. Lambeck, M. I. Bird, and J. O. Stone, The history of the Antarctic ice sheet from Holocene sea level change, *Eos Trans. AGU*, *77*(22), West. Pac. Geophys. Meet. Suppl., W12–W13, 1996.

S. Bannister, Institute of Geological and Nuclear Sciences, P.O. Box 1320, Wellington, New Zealand. (e-mail: stephen@piopio.gns.cri.nz)

R. I. Hackney, Department of Geology and Geophysics, University of Western Australia, Nedlands, Western Australia 6009, Australia. (e-mail: rhackney@mail.geol.uwa.edu.au)

Y. Makovsky, Geophysics Department, Stanford University, Stanford, CA 94305. (e-mail: yizhaq@moho.stanford.edu)

T. A. Stern, Institute of Geophysics, Victoria University of Wellington, P.O. Box 600, Wellington, New Zealand. (e-mail: tim.stern@vuw.ac.nz)

U. S. ten Brink, U.S. Geological Survey, Quissett Campus, Woods Hole, MA 02543-1598. (e-mail: utenbrink@amg.er.usgs.gov)

(Received February 11, 1997; revised August 25, 1997; accepted September 2, 1997.)